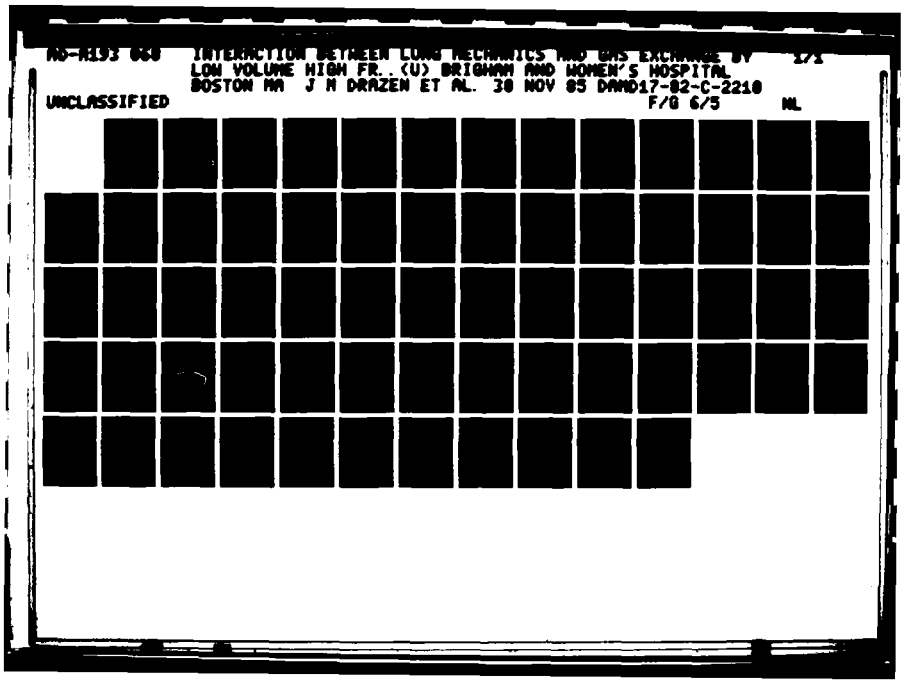
AD-A193 868 INTERACTION BETWEEN LUNG MECHANICS AND GAS EXCHANGE BY 1/1
LOW VOLUME HIGH FR..(U) BRIGHAM AND WOMEN'S HOSPITAL
BOSTON MA J M DRAZEN ET AL. 30 NOV 85 DAMD17-82-C-2218
UNCLASSIFIED F/G 6/5 NL

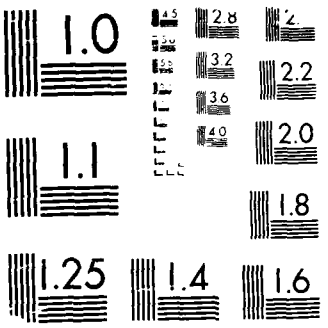

MICROCOPY RESOLUTION TEST CHART

AD_____

Interaction between Lung Mechanics and Gas Exchange by Low Volume High Frequency Pulmonary Ventilation in Patients with Respiratory Failure

Annual Summary Report

Jeffrey M. Drazen, M.D., Phillip Drinker, Ph.D., Thomas Rossing, M.D.
Julian Solway, M.D., Roger D. Kamm, Ph.D., Ishmail Dreshai, M.D.
and Rayhana Akhaven

November 30, 1985

Supported by

U.S. ARMY MEDICAL RESEARCH AND DEVELOPMENT COMMAND
Fort Detrick, Frederick, Maryland 21701-5012

Contract No. DAMD17-82-C-2210

Brigham and Women's Hospital
75 Francis Street
Boston, Massachusetts 02115

DOD Distribution Statement

Approved for public release; distribution unlimited

SECURITY CLASSIFICATION OF THIS PAGE

ADA193068

REPORT DOCUMENTATION PAGE

1a. REPORT SECURITY CLASSIFICATION Unclassified	1b. RESTRICTIVE MARKINGS
2a. SECURITY CLASSIFICATION AUTHORITY	3. DISTRIBUTION / AVAILABILITY OF REPORT
2b. DECLASSIFICATION / DOWNGRADING SCHEDULE	
4. PERFORMING ORGANIZATION REPORT NUMBER(S)	5. MONITORING ORGANIZATION REPORT NUMBER(S)
6a. NAME OF PERFORMING ORGANIZATION Brigham & Women's Hospital 6b. OFFICE SYMBOL (If applicable)	7a. NAME OF MONITORING ORGANIZATION
6c. ADDRESS (City, State, and ZIP Code) 10 Vining Street Boston, MA 02115	7b. ADDRESS (City, State, and ZIP Code)
8a. NAME OF FUNDING / SPONSORING ORGANIZATION U.S. Army Medical Research & Development Command 8b. OFFICE SYMBOL (If applicable)	9. PROCUREMENT INSTRUMENT IDENTIFICATION NUMBER DAMD17-82-C-2210
8c. ADDRESS (City, State, and ZIP Code) Fort Detrick Frederick, Maryland 21701-5012	10. SOURCE OF FUNDING NUMBERS PROGRAM ELEMENT NO. 62734A PROJECT NO. 3MI62734A875 TASK NO. CC WORK UNIT ACCESSION NO. 336

11. TITLE (Include Security Classification)
Interaction Between Lung Mechanics and Gas Exchange by Low Volume High Frequency Pulmonary Ventilation in Patients with Respiratory Failure

12. PERSONAL AUTHOR(S)
Jeffrey Drazen, M.D.

13a. TYPE OF REPORT	13b. TIME COVERED	14. DATE OF REPORT (Year, Month, Day)	15. PAGE COUNT
Annual	FROM 10/1/84 TO 9/30/85	85 November 30	

16. SUPPLEMENTARY NOTATION

17. COSATI CODES			18. SUBJECT TERMS (Continue on reverse if necessary and identify by block number)
FIELD	GROUP	SUB-GROUP	High Frequency Ventilation Mechanical Ventilation
15	06		
06	11		

19. ABSTRACT (Continue on reverse if necessary and identify by block number)

Flow limitation during a forced expiration was simulated by a mathematical model. This model draws upon a pressure-area law obtained in other work, and on known methods of analysis for flow in collapsible tubes. This approach represents an improvement over previous models in that (i) the effects of changing lung volume and of parenchymal/bronchial interdependence are simulated, (ii) a more realistic representation of the collapsed airways is employed, (iii) a solution is obtained mouthward of the flow limiting site by allowing for a smooth transition from subcritical to supercritical flow speeds, then matching mouth pressure by imposing an elastic jump (an abrupt transition from supercritical to subcritical flow speeds) at the appropriate location, and (iv) the effects of levels of effort (or vacuum pressure) in excess of those required to produce incipient flow limitation are examined, including the effects of potential physiological limitation.

20. DISTRIBUTION / AVAILABILITY OF ABSTRACT	21. ABSTRACT SECURITY CLASSIFICATION	
☐ UNCLASSIFIED/UNLIMITED ☐ SAME AS RPT. ☐ DTIC USERS		
22a. NAME OF RESPONSIBLE INDIVIDUAL Mrs. Virginia Miller	22b. TELEPHONE (Include Area Code) 301/663-7325	22c. OFFICE SYMBOL SGRD-RMS

DD FORM 1473, 84 MAR 83 APR edition may be used until exhausted. All other editions are obsolete.

SECURITY CLASSIFICATION OF THIS PAGE

In patients, dynamic hyperinflation of the lungs occurs during high frequency oscillatory ventilation (HFOV), and has been attributed to asymmetry of inspiratory and expiratory impedances. To identify the nature of this asymmetry, we compared changes in lung volume (V_L) observed during HFOV in ventilator-dependent patients with predictions of V_L changes from electrical analogs of 3 potential modes of impedance asymmetry. In the patients when a fixed oscillatory tidal volume was applied at a low mean airway opening pressure (Pao) which resulted in little increase in FRC, progressively greater dynamic hyperinflation was observed as HFOV frequency (f) was increased. When mean Pao was raised such that resting V_L increased, V_L remained at this level during HFOV as f was increased, until a critical f was reached; above this value, V_L increased further with f in a fashion nearly parallel to that observed when low mean Pao was used. Three modes of asymmetric inspiratory and expiratory impedance were modelled as electrical circuits: (a) fixed asymmetric resistance [Rexp > Rinsp]; (b) variable asymmetric resistance [Rexp(V_L) > Rinsp, with Rexp(V_L) decreasing as V_L increased; and (c) equal Rinsp and Rexp,1 but with superimposed expiratory flow limitation, the latter simulated using a bipolar transistor as a descriptive model of this phenomenon. The fixed and the variable asymmetric resistance models displayed a progressive increase of mean V_L with f at either low or high mean Pao. Only the expiratory flow limitation model displayed a dependence of dynamic hyperinflation on mean Pao and f similar to that observed in our patients. We conclude that expiratory flow limitation can account for dynamic pulmonary hyperinflation during HFOV.

FOREWORD

Citations of commercial organizations and trade names in this report do not constitute an official Department of the Army endorsement or approval of the products or services of these organizations.

For the protection of human subjects, the investigator(s) have adhered to policies of applicable Federal Law 45CFR46.

Table of Contents

I. SUMMARY

Flow limitation during a forced expiration was simulated by a mathematical model. This model draws upon a pressure-area law obtained in other work, and on known methods of analysis for flow in collapsible tubes. This approach represents an improvement over previous models in that ~~(i)~~ the effects of changing lung volume and of parenchymal/bronchial interdependence are simulated, ~~(ii)~~ a more realistic representation of the collapsed airways is employed, ~~(iii)~~ a solution is obtained mouthward of the flow limiting site by allowing for a smooth transition from subcritical to supercritical flow speeds, then matching mouth pressure by imposing an elastic jump (an abrupt transition from supercritical to subcritical flow speeds) at the appropriate location, and ~~(iv)~~ the effects of levels of effort (or vacuum pressure) in excess of those required to produce incipient flow limitation are examined, including the effects of potential physiological limitation.

In patients, dynamic hyperinflation of the lungs occurs during high frequency oscillatory ventilation (HFOV), and has been attributed to asymmetry of inspiratory and expiratory impedances. To identify the nature of this asymmetry, we compared changes in lung volume (V_L) observed during HFOV in ventilator-dependent patients with predictions of V_L changes from electrical analogs of 3 potential modes of impedance asymmetry. In the patients when a fixed oscillatory tidal volume was applied at a low mean airway opening pressure (Pao) which resulted in little increase in FRC, progressively greater dynamic hyperinflation was observed as HFOV frequency (f) was increased. When mean Pao was raised such that resting V_L increased, V_L remained at this level during HFOV as f was increased, until a critical f was reached; above this value, V_L increased further with f in a fashion nearly parallel to that observed when low mean Pao was used. Three modes of asymmetric inspiratory and expiratory impedance were modelled as electrical circuits: (a) fixed asymmetric resistance [Rexp > Rinsp]; (b) variable asymmetric resistance [$R_{exp}(V_L)$ > Rinsp, with $R_{exp}(V_L)$ decreasing as V_L increased; and (c) equal Rinsp and Rexp,1 but with superimposed expiratory flow limitation, the latter simulated using a bipolar transistor as a descriptive model of this phenomenon. The fixed and the variable asymmetric resistance models displayed a progressive increase of mean V_L with f at either low or high mean Pao. Only the expiratory flow limitation model displayed a dependence of dynamic hyperinflation on mean Pao and f similar to that observed in our patients. We conclude that expiratory flow limitation can account for dynamic pulmonary hyperinflation during HFOV.

III. OVERALL INTRODUCTION

During year 03 of this contract we performed both hardware model experiments and patient studies. Each will be addressed separately.

1. INTRODUCTION

A forced expiration maneuver, as characterized by a Maximal Expiratory Flow Volume (MEFV) curve has long been used as a test of pulmonary function. (See Hyatt (1983) for an extensive review.) The MEFV curves produced by a given subject are highly reproducible, but can vary markedly among different subjects even when an adjustment is made to correct for differences in lung volume (Green et. al., 1974). Consistent and characteristic differences in the shape of the MEFV curve are found among different species (Macklem et. al., 1968) and depending on whether the forced expiration is produced by respiratory effort or by lowering mouth pressure (reference).

The repeatibility of the MEFV curve in a particular subject is often attributed to flow limitation; that the flow rate produced at constant lung volume is insensitive to further changes in respiratory effort when the former reaches some critical level. For lung volumes from about 30% to 70% of Total Lung Capacity (TLC) this is generally thought to be due to wave speed limitation which occurs when the flow velocity equals the wave speed at some location in the airways. The point at which these speeds are equal (termed the Flow Limiting Site (FLS)) is apparently found in the trachea at high lung volumes, then progresses upstream (toward the periphery) as lung volume decreases (Smaldone et al., 1976; Hyatt etal., 1980; Pedersen et al., 1982), but probably resides in the central airways even at low lung volumes (Smaldone and Smith, 1985). While these arguments seem essentially correct for most lung volumes, at lung volumes greater than about 70% TLC, maximum flow is determined instead by physiological limitation of the expiratory muscles (Hyatt et al., 1966; Mead et al., 1967) in which case expiratory flow is observed to be effort dependent (Mead et al,1967).

Recently, experimental methods have been developed to determine the location of the FLS in excised and intact canine and human lungs. In these studies, the FLS is taken to be the furthest mouthward point at which lateral pressure, at a certain lung volume, remains constant while mouth pressure is lowered in successive expirations. Most evidence suggests that the FLS first forms in the trachea, then progresses upstream (peripherally), with decreasing lung volume.

The nature of flow limitation has also been examined through experiments using different gas mixtures. The MEFV curves are found to depend primarily upon gas density at high lung volumes, but become increasingly sensitive to gas viscosity as lung volume decreases. The relative effects of different gases on the location of the FLS has not been clearly established (Wood et al., 1976; Mink et al., 1979; Staats et al., 1980).

These observations, and the desire to better understand the mechanistic basis for flow limitation, provided the impetus to develop models to simulate a forced expiration. The most recent and most rigorous of these models is that of Lambert and Wilson . In their model, the lung is treated as a symmetric branching network with distributed properties. Flow calculations proceed from the alveolar zone toward the mouth using differential forms of the mass and momentum conservation equations in conjunction with a constitutive relation between tranpulmonary pressure and cross-sectional area (the "tube law"). Flow limitation is attained by incrementing the flow at the upstream (alveolar) end of the system until reaching a state is reached for which the flow speed and wave speed become equal at some point in the network (the FLS). While their model reproduces many features of a forced expiration, it cannot be used to examine flows downstream of the FLS. Further, the airway constitutive relation used in their study is based on limited data obtained by uniform lung inflation at positive distending pressures and fails to take into account the effects of parenchyma/bronchial interdependence or changes in lung volume.

A more general approach to steady flow in collapsible tubes was developed by Shapiro (1977). Starting with the equations of mass and momentum conservation and the tube law for the vessel, the analysis shows how the area ratio ($\alpha \equiv A/A_o$ where A_o is some reference cross-sectional area) and the speed index (S, the ratio between flow velocity and the local speed of long waves) vary with streamwise distance. This formulation more clearly identifies the different characters of sub-critical ($S<1$) and super-critical ($S>1$) flow and allows one to examine possible transitions between these two states.

In a previous work (Elad et al., 1985) we employed this same approach to investigate various types of flow in a lung-like model. Solutions were obtained which contained a smooth sub- to super-critical transition, followed by a "shock-like" deceleration (an "elastic jump") back to sub-critical speed. The location and strength of the elastic jump provided solutions which matched "mouth" pressure downstream. These studies, while qualitatively similar to flows during a forced expiration, were conducted for the primary purpose of exploring different types of flow behavior. Accordingly, no attempt was made to mimic all important aspects of the respiratory system.

In the present investigation we employ the same principles to a model which more closely simulates the lung. This model allows us to calculate flow conditions beyond the FLS, an essential step toward the development of models incorporating airway asymmetry. We also consider the conditions that exist when respiratory effort exceeds the minimum value necessary to produce flow limitation and demonstrate how the occurance of

"elastic jumps" allows the flow solution to match the downstream pressure existing at the mouth.

These calculations incorporate a tube law based on experimental results in which bronchial pressure is varied while alveolar pressure is held constant. This tube law provides for a more realistic representation of the effects of parenchymal tensions and of changing lung volume as the forced expiration proceeds to completion.

The differences and similarities between forced expiration and forced evacuation are examined as are the effects of small perturbations from a monotonic variation in airway stiffness or area, as might exist in various respiratory disorders.

2. BASIC CONCEPTS OF THE MODEL

The Tube Law

In Elad et al (1985), a generalized, self-similar tube law was obtained, based on the premise that the fundamental character of collapse at different lung volumes is essentially the same. Accordingly, we found that an appropriately chosen dimensionless form of the pressure-area relationship remains valid over a broad range of lung volumes. This relationship was expressed in the form:

$$\Pi = \frac{(P_{br}-P_{alv})-P_0}{K} = \alpha^{0.5} - \alpha^{-0.2} \qquad (1)$$

where

$$\alpha = A/A_0 \qquad (2)$$

Here, P_{br} is the internal bronchial pressure, P_{alv} the alveolar pressure, A the cross-sectional area of a single airway, A_0 and P_0 are the cross-sectional area and the pressure difference ($P_{br}-P_{alv}$) at the inflection point of the pressure-area curve, and K is the effective wall stiffness. In Elad et al (1985), A_0, P_0, and K were shown to depend upon a dimensionless lung volume, λ, defined by

$$\lambda = V_L/V_{LO} \qquad (3)$$

where V_L is lung volume and V_{LO} a reference volume corresponding to 35% of TLC (Klingele et al., 1971; Hughes et al., 1972).

We now need to generalize from the tube law of Elad et al (1985) (which was based on data from a single airway generation) to one which is applicable to the entire airway system. Again we start with the assumption that the mechanics of airway collapse is basically the same regardless of airway size or location in the lung. Therefore, we anticipate the existence of a universal tube law, of the same basic form of equation (1), but in which the parameters which characterize the stiffness and size of the airway vary as a function of airway generation. Thus we take K, P_0, and A_0 to be functions of <u>both</u> lung volume and distance along the branching network. Assuming the dependence on lung volume to be of the same form for all airways, we carry over the results of Elad et al (1985):

$$P_0 = P_{00}(\xi)\ [0.0136\ (\lambda^{7.4} - 1)] \tag{4}$$

$$A_0 = A_{00}(\xi)\ [1.0 + 0.01345\ (\lambda^{2.7} - 1)] \tag{5}$$

$$K = K_0(\xi)\ [\ 1.0 + 0.078\ (\lambda^{2.7} - 1)] \tag{6}$$

where $P_{00}(\xi)$ and $A_{00}(\xi)$ are, respectively, the distributions of pressure and cross-sectional area at the inflection point of the pressure-area tube law for lung volume V_{LO}, $K_0(\xi)$ is similarly the distribution of effective wall stiffness at V_{LO}, and $\xi = x/L$ is a nondimensional length, normalized by the total length L of the conducting system up to the 17th generation.

<u>Changes Along the Airway Network</u>

According to the discussion of Elad et al (1985), A_0 represents the distribution of area at the inflection point of the tube law for that lung volume at which the parenchyma exerts no external tethering force, a value assumed earlier to be equal to V_{LO}. In order to use the morphological data of Weibel (1963), which was obtained from a lung inflated to 75% TLC, we need to adjust down to V_{LO} (35% TLC), taking into account the associated changes in airway length. For this purpose, we assume that the length of each airway is constant for changes at constant lung volume, but varies as the cube root of the volume ratio (Hughes et al., 1972). Hence

$$L = L_{00}\lambda^{1/3} \tag{7}$$

where L_{00} is the length of the vessel at V_{LO}. Taking into account both the change in lung volume and the length correction gives

$$A_{00}(\xi) = 0.916\ A_W(\xi) \tag{8}$$

where $A_W(\xi)$ is the area distribution of Weibel (1963) given later in equation (9).

It is somewhat more difficult to obtain accurate estimates for the two parameters affecting airway stiffness, K and P_{OO}. Many observations confirm that the peripheral airways are most compliant and that the airways become progressively stiffer moving toward the trachea. There are, however, no data available from which we can determine the precise nature of this distribution. Hence, we assume that the effective wall stiffness at V_{LO}, varies exponentially along the bronchial tree, according to

$$K_O(\xi) = K_{OO} \exp(C_k \xi) \qquad (11)$$

where K_{OO} is the effective wall stiffness of the most peripheral generation (generation 17 in the present model) at V_{LO}, and C_k is an empirical constant that controls the relative change along the bronchial generations.

We obtain one value for K from the data analysis of Elad et al (1985), and set $K(\xi=0.33,\lambda=1) = 37.1$ cmH_2O (data from the third generation of Dog 20). Since no data of comparable form exist for airways from other generations, we consider instead the experimental results of Martin et al., (1958), obtained from three excised bronchi: trachea, 5mm and 2mm outside diameter. Noting that the 2mm airway is roughly 6 times as compliant as the trachea we obtain C_k=2.40 which, in turn, dictates that K_{OO} = 16.7cmH_2O.

Finally, we need to specify the variation in P_O. Here, for lack of empirical data on which to rely, we assume that P_O/K is independent of ξ (i.e., P_O varies exponentially) for reasons of geometric and structural similarity.

Airway System Geometry

For the purpose of the present model, the bronchial tree is represented as a continuously branching symmetric network with a monotonic increase of the total cross-sectional area (Fig.1) based on the morphometric data of Weibel (1963), obtained from a human lung inflated to 75% of TLC. The complex geometry with discrete bifurcations is replaced by a continous one-dimensional model in which the number of the bronchi and their diameter at each generation is represented by smooth and continuous functions of distance along the bronchial tree.

We describe the total cross-sectional area (A) and number of branches (N) using hyperbolic functions with an exponential correction term, fitted to Weibel's data. The result is shown in Fig 2., and is given by:

$$A_w(\xi) = 2.3255(\xi+0.01)^{-0.9} - 14.0\exp(-3.9844\xi) \qquad (9)$$

$$N_w(\xi) = 1.0387(\xi+0.01)^{-2.4} - 50.0\exp(-5.9766\xi) \qquad (10)$$

Also, from Weibel, we find that L = 26.5 cm at 75% TLC, or 20.6 cm at our reference state according to equation (2). The local diameter of a single tube at a given lung volume is given by

$$D_0(\xi) = \left[\frac{4A_0(\xi)}{\pi N(\xi)}\right]^{1/2}$$

Conservation of Mass and Momentum

Consistant with other investigations (e.g. Lambert and Wilson), we assume that flow during a forced expiration can be described by a series of quasi-steady states at progressively decreasing fixed lung volumes. This is justified by the fact that the characteristic time for a forced expriation is much larger than both the time required for waves to propagate along the bronchial tree and for a fluid particle to traverse the branching network. We consider a one-dimensional flow with wall friction in a multi-channel network. External pressure is assumed to be equal to alveolar pressure, as described in Elad et al (1985). We later examine the effect of a gradient in external pressure at the transition between the intrapulmonary and extrapulmonary airways. With these assumptions, we can write the equations for mass conservation:

$$uA = \text{constant} \tag{12}$$

and conservation of momentum

$$u\frac{\partial u}{\partial x} + \frac{1}{\rho}\frac{\partial P_{br}}{\partial x} + \frac{\tau_w s}{\rho A} = 0 \tag{13}$$

where s is the airway perimeter, τ_w the shear stress at the wall, u the cross-sectional average gas velocity, A the cross-sectional area of the tube, ρ the gas density and x the longitudinal coordinate.

Frictional Dissipation

The shear stress is expressed as $\tau_w = \rho u^2 f_T/2$ where f_T is the friction coefficient. The friction coefficient is determined from Reynolds (1982), who measured the <u>total</u> frictional loss due to water flow in a latex model of the first 10 generations of a human bronchial tree. Based on his experimental results, and an assumed distribution of loss among the generations, he proposed the following formula for the <u>local</u> frictional pressure drop:

$$\Delta P = (a + b\ Re)\ \Delta P_p \tag{14}$$

where ΔP_p is the Poiseuille pressure drop $8\pi\mu QL/A^2$, Re is the Reynolds number ($R_e = uD_e/\nu$ where ν is the kinematic viscosity experimental data (a = 1.9, b = 0.0035). This result can also be expressed in terms of the friction coefficient:

$$f_T = \frac{16}{Re}\ (a + b\ Re) \tag{15}$$

which exhibits laminar flow behavior when Re is small and takes on the character of turbulent flow when Re is large.

We have chosen to use this relation in a slightly modified form, using b = 0.0013 rather than 0.0035 as given by Reynolds. The value given by Reynolds for b is roughly four times that found in fully developed turbulent flow through a moderately rough straight tube. Based on the recognition that (i) Re at the point of greatest frictional loss is of order 10^2, and (ii) that the airways where this loss occurs are likely to be partially collapsed and therefore of a different cross-sectional shape from the airways tested by Reynolds, we use the lower value given above. Later, in the Discussion, we examine the effect of varying both a and b on the simulation results.

Dimensionless Governing Equations

Normalized relationships can be obtained by introducing the speed index, S=u/c, the area ratio α defined in equation (2), a normalized alveolar pressure $\Pi_{alv}=P_{alv}/K$, and the non-dimensional length $\xi=x/L$. The resulting expressions are similar to those obtained in our previous work (Elad et al. 1985b)

$$\frac{d\alpha}{d\xi} = \frac{\alpha}{1-S^2}\left[\frac{S^2}{A_0}\frac{dA_0}{d\xi} - \frac{1}{\alpha}\frac{d\Pi_{alv}}{d\xi} - \frac{2S^2 f_T L}{\alpha D_0} - \frac{\Pi + \Pi_{alv}}{\alpha\Pi'}\frac{1}{K}\frac{dK}{d\xi}\right] \tag{16}$$

$$\frac{dS^2}{d\xi} = \frac{S^2}{1-S^2}\left[\frac{-2+(2-M)S^2}{A_0}\frac{dA_0}{d\xi} + \frac{M}{\alpha}\frac{d\Pi_{alv}}{d\xi} + \frac{2MS^2 f_T L}{\alpha D_0} + \right. \tag{17}$$

$$\left. + \left[M\frac{\Pi + \Pi_{avl}}{\alpha\,\Pi'} - (1-S^2)\right]\frac{1}{K}\frac{dK}{d\xi}\right]$$

where $\Pi' = d\Pi/d\alpha$ and $M = \alpha\Pi''/\Pi'$. This presentation highlights the separate effects associated, respectively, with variations in rest area, variations in external (alveolar) pressure, friction, and variations in wall stiffness represented by the first through fourth terms on the RHS of each expression.

It can be seen that mathematical singularities appear when S=1 since the denominator on the RHS of both expressions goes to zero. It has been shown (Shapiro, 1977, Elad et al, 1985b) that one of two situations can exist when S=1. If the numerator passes through zero at precisely the same point at which S=1 then a smooth and continuous transition from subcritical to supercritical speed is possible. This can occur in a variety of ways. Consider, for example, the case in which only the first term on the RHS of equations (16) and (17) is important, that associated with variations in A_o. A smooth transition in this instance can result only when A_o passes through a local minimum ($dA_o/d\xi = 0$) when S = 1. Under more general circumstances such as are found in the lung, all the terms on the RHS contribute, but their sum must still pass through zero when S=1 in order to allow a smooth transition. While it would seem to be difficult to achieve such a singular condition, it proves to be relatively easy to produce smooth sub-to supercritical transitions in laboratory experiments.

If, on the other hand, the numerator on the RHS does <u>not</u> pass through zero when S=1, a different situation exists, termed a "choke point." At a choke point, since the numerator is non-zero, the derivatives $dS^2/d\xi$ and $d\alpha/d\xi$ are infinite in magnitude when S reaches 1. For related reasons, it is not possible to continue the mathematical solution downstream, beyond a choke point. Hence, in a real flow, a choke point can only occur at the end of the airway system. A FLS must therefore be a sub- to super-critical transition point rather than a choke point.

This raises a question concerning the nature of flow downstream of the transition or FLS. Following a smooth transition to S>1, the flow is supercritical for some distance. In laboratory experiments , this super-critical zone can be terminated in an 'elastic jump' if the downstream pressure is too high; this is a shock-like transition back to subcritical speed associated with a relatively abrupt increase in area and pressure. Elastic jumps have been the subject of several modeling efforts which have arrived at the following description. Application of conservation of mass and momentum for the region containing the elastic jump, produces the result that the quantity

$$\Phi(A) \equiv \frac{Q^2}{A} + \int_A \frac{A}{\rho} \frac{d(P_{br} - P_{alv})}{dA} dA \qquad (18)$$

has the same value at both ends of the elastic jump .

Boundary Conditions

The physics of a forced expiration is controlled by Eqs. (18) and (19) which include the fluid flow dynamics (Eqs. (16) and (17)) and the tube wall properties (Eqs.(6), (7), (8), (9), (10), (11)) and can be integrated numerically for given boundary conditions. In the case of a forced expiration mouth pressure (at ξ=1) equals atmospheric pressure. At the periphery (ξ=0), the bronchi merge into the alveolar zone. Consequently the boundary conditions are:

$$\xi=0 \qquad P_{br}=P_{alv} \tag{19}$$

$$\xi=1 \qquad P_{br} = P_{atm} + \Delta P_g$$

where P_{atm} is atmospheric pressure and ΔP_g is the pressure drop across the glottis and mouth.

To determine ΔP_g, we use the results of Jaeger et al. (1969) who demonstrated that upper airway resistance, from mid-trachea to the mouth, can be described over the Reynolds number range Re=10 to 10^4 by a nondimensional loss coefficient:

$$C_d = \frac{Q}{A}\left(\frac{\rho}{2\Delta P_g}\right)^{1/2} \tag{20}$$

We fitted Jaeger's result for C_d to an analytic function of Reynolds number (shown in Fig. 3) given by

$$\ln C_d = -3.394 + 0.776 \ln_3 Re - 0.0495 (\ln Re)^2 + 0.000813 (\ln Re)^3 \tag{21}$$

where we have assumed, as did Jaeger et al , that cross-sectional area at the glottis is approximately 1.0 cm^2.

In addition, it has been shown that the resistance of the upper airways, including glottis and mouth, decreases with increasing lung volume (Hyatt et al., 1961; Wilson 1969; Stanescu et al., 1972). For the present work we assume that the lung volume dependence is of the form of $\Delta P_g/Q=1.5/\lambda$ which is roughly consistent with experimental observation. The final expression for the pressure drop across the glottis and the mouth becomes

$$\Delta P_g = \frac{1}{C_d^2}\,\frac{\rho u_2}{2}\,\frac{1.5}{\lambda} \tag{22}$$

Numerical Procedure

As noted above the FLS is a transition point corresponding to S=1. Setting S = 1 in Eqs. (16) and (17) gives rise to a mathematical singularity in that the denominator of both expressions goes to zero. For a mathematical solution to exist on both sides of this singular point, it is necessary that the denominator of both expressions also equal zero when S=1; consequently $d\alpha/d\xi=dS^2/d\xi=0/0$. Only under these conditions can a continuous solution exist which causes the flow to accelerate from S<1 to S>1. One can calculate all possible singular (transition) points by setting the numerators of the right-hand side of Eqs. (16) and (17) (which are identical for S=1) to zero while S=1. This yields a locus of possible transition points, for each lung volume, as shown in Fig. 4. A transition curve for each lung volume and ξ^* may be found by integrating Eqs. (16) and (17) from the critical point (ξ^*) to the upstream end (ξ=0). The relevent curve for a particular lung volume, found by trial and error, is that for the value of ξ^* that satifies the boundary condition $P_{br}=P_{aly}$ at ξ=0. These values of ξ^* representing the flow conditions are indicated by the open circles (corresponding to each of several different lung volumes) on the curves of Fig. 4. Having identified the FLS, one can easily calculate the critical flow rate (maximum flow rate) for a given lung volume. Then, by integration of Eqs. (18) and (19), both upstream and downstream (curves A and B, respectively, in Fig. xx), we can obtain $S(\xi)$ and $\alpha(\xi)$ for each lung volume.

Selection of the transition point as shown above insures that the upstream boundary condition will be satisfied. But this procedure generally leads to some pressure other than mouth pressure at ξ=0. To satisfy the downstream boundary condition of pressure requires a trial and error procedure. First we integrate eqns. (18) and (19) to get $S(\xi)$ and $\alpha(\xi)$in the upstream direction, starting from ξ=1 where we know both the flow rate and the local (mouth) pressure. This yields curve C in Fig. xx. We then attempt to fit elastic jumps, as characterized by equation (18), to bridge between the two solution curves B and C. The actual location of the elastic jump ξ_e is that point at which the jump conditions match curves B and C.

3. RESULTS

The location of the FLS and the maximum flow rates for several lung volumes are shown in Fig. 5. The different symbols correspond to several different combinations of friction and stiffness coefficients.

Figures 6a and 6b illustrate the distribution of area ratio (α) and speed index (S), respectively, along the continuous branching network. Each curve corresponds, for example, to a different level of respiratory effort; those curves for which S

either reaches or exceeds one are flow limited. Note that all area ratios are less than one (in the "collapsed" portion of the tube law).

The critical flow curve (corresponding to the maximum flow rate for given lung volume) can have either a subcritical or a supercritical branch downstream of the FLS, depending on pressure at the mouth (ξ=1). Supercritical branches either remain supercritical to the end of the network (ξ = 1) or undergo a transition to S<1 by means of an elastic jump, a shock-like transition from supercritical to subcritical flow speed, as described above.

Fig. (6c) shows the results for evacuation of a lung by applying vacuum at the mouth. In this case upstream pressure is held fixed and mouth pressure is reduced. Pressure progressivley falls toward the mouth, reaching a local minimum at some point downstream of the FLS.

The pressure curves can also be plotted to simulate forced expiration produced by respiratory effort by simply shifting all the curves in Fig. (6c) vertically, so that $P_{mouth}-P_{atm}=0$ as shown in Fig. 6(d) (and as described in the Discussion). The latter curves represent forced expirations performed at different levels of muscular effort producing different upstream conditions.

An important feature of flows with elastic jumps is that the amount of energy dissipated in the region mouthward from the FLS can vary depending upon the location of the jump. This occurs in two ways: first, the frictional dissipation due to wall shear stress varies depending on the relative lengths of supercrictical and subcritical flow; and second, the dissipation associated with the jump itself depends on conditions upstream of the jump. Thus, it becomes possible to attain different pressures at the mouth, for identical flows upstream of the FLS, by changing the position of the jump. Reductions in mouth pressure cause the elastic jump to move progressively mouthward while leaving the flow rate exiting from the lung unchanged.

Plotting driving pressure, $P_{aly}-P_{atm}$, from the different curves of Fig. 6(d) against the corresponding flow rate, at fixed lung volume, yields the Iso-Volume Pressure Flow (IVPF) curves shown in Fig. 7. The critical driving pressure, $P_c=P_{aly}-P_{atm}$, required to achieve flow limitation is indicated on each IVPF curve in Fig. 7 and plotted as a function of lung volume in Fig. 9 for several different conditions.

The model is also used to calculate the MEFV curves and flow limitation sites for different gases as shown in Fig. 8.

4. DISCUSSION

General Character of the Results

The maximal flow rate and the location of flow limiting sites, predicted by the present model, are summarized in Fig. 5, together with some representative experimental data. The agreement is generally good although the flow-volume pattern obtained by simulation appears to be better matched to the canine experiments than the human experiments. There are several possible explanations for this. First, since the data we used to produce our pressure-area law was obtained from dogs, we might expect the predictions to exhibit some features of a canine flow-volume curve. Second, if the difference in shape of the MEFV curve is due to variations in tracheal tension, as suggested by Smaldone and Smith (1985), then it would be difficult for any model not incorporating such effects to distinguish one pattern from the other. Yet another possibility, related to uncertainties in selecting some of the parameters of the model, is discussed later.

The pressure distributions of Fig. 6 are of particular interest in view of several inferences drawn from experimental measurements. As mentioned in the Introduction, it is generally held that the FLS is the furthest mouthward point which is insensitive to changes in downstream pressure. In Fig. 6(c) the FLS is identified by the closed circle (ξ=0.56) and flow limitation is attained for mouth pressures more than 59 cm H_2O below alveolar pressure. As mouth pressure falls below this value, the region within which pressure is insensitive to changes in mouth pressure expands some distance downstream of the FLS, producing a region of supercritical flow ($S>1$) terminated by an elastic jump. The point identified experimentally as the FLS would, according to these results, be the location of the elastic jump rather than the location where wave speed exceeds flow speed ($S=1$);it would therefore vary depending upon the values of mouth pressure used in the experiments.

The curves in Fig. 6 can also be compared to the area and pressure distributions of Lambert and Wilson (LW) (their Fig. 11). Whereas area and pressure experience a relatively smooth transition through the FLS in our calculations, it appears that the spatial derivatives of both area and pressure become extremely steep (perhaps approaching infinity) in the calculations of LW. This is at least suggestive of a choke point singularity as opposed to a smooth transition; if so, it would therefore lead, in their calculations, to a solution which cannot be mathematically continued downstream of the FLS and which is therefore physically impossible. In practical terms, it would signify that they had overestimated the maximum flow possible.

Equivalency Between Expiration and Evacuation

During a natural forced expiration, gas is driven mouthward due to contraction of the expiratory muscles and the muscles of the diaphragm producing pleural pressures much in excess of

atmospheric pressure At each lung volume, alveolar pressure exceeds pleural pressure by the elastic recoil pressure (P_{ER}), which depends on lung volume. In experimental investigations with anesthetized dogs or with excised lungs, a forced expiration is produced by evacuation of the lung by means of a vacuum applied at the mouth or at the tracheal exit. That these two expiratory maneuvers are essentially equivalent, can be substantiated by the following line of reasoning.

As discussed earlier, the flow occuring at a particular lung volume during a forced expiration is equivalent to a steady flow at the same lung volume, calculated as though alveolar volume remained constant. With this assumption incorporated into the model, the flow rate through the bronchial system (and, indeed, the entire solution) is found to depend only upon the transmural pressures acting at the upstream (ξ=0) and downstream (ξ=1) end. Since upstream (peripheral) transmural pressure is fixed ($P_{br}=P_{alv}$ at ξ=0), flow rate is only a function of downstream transmural pressure. Noting that $P_{alv}=P_{pl}+P_{ER}$ and $(P_{br})_{\xi=1}=\Delta P_g+P_{atm}$, the downstream transmural pressure can be written as $(P_{br}-P_{alv})_{\xi=1} = (P_{atm}+\Delta P_g-P_{pl}-P_{ER})$ where ΔP_g is the pressure drop across the glottis and mouth; a constant value for a given flow and lung volume. Since fixed values for this expression yield the same flow rate, it can be seen that the effect of increasing pleural pressure with mouth pressure fixed, by changing expiratory effort, is entirely equivalent to the effect of holding pleural pressure fixed and reducing mouth pressure below atmospheric by means of vacuum provided the magnitude of pressure change in each instance is the same.

This conclusion, however, is not necessarily true if the critical point lies in the region where the "external" pressure on the airway varies because the latter passes out of the thoracic cavity.

Breathing Different Gases

Experimental measurements have demonstrated that MEFV curves differ for different gases at high and moderate lung volumes, but tend to merge near end expiration (Wood et al. 1976, Mink et al., 1979). We used the present model to predict flows for a mixture of 80% He and 20% O_2 and a mixture of 80% SF_6 and 20% O_2. The results for these mixtures and air are shown in Fig. 8. While the general trend of the maximal flow curve is as expected (the difference at a given lung volume varies as the square root of the density), a somewhat greater density dependence is predicted than is observed experimentally, particularly at low lung volumes.

These differences between the present calculations and experimental results may be due to a stronger dependence on gas viscosity in the lung than predicted by the model and may be associated with the differences in maximal flow at low lung

volume noted earlier. It may also be related to deficiencies in the tube law for the peripheral airways, where there is a paucity of experimental data.

The location of the FLS is seen also to depend on gas properties and tends to move downstream (mouthward) when gas density is reduced.

The Effect of Variations in External Pressure

Up to this point we have assumed that the effective external pressure for all the bronchial airways is uniform and equal to alveolar pressure. This assumption is not strictly true and may in fact be a very poor approximation in the extra-pulmonary bronchi and the extra-thoracic trachea. It is possible, however, to relax this constraint in the model and consider the implications of variations in effective external pressure.

To examine these effects we change the model and assume that all intrathoracic bronchi are exposed to the same uniform external pressure (extra-pulmonary but introthoracic bronchi are enclosed by the lobes of the lung and are therefore probably subjected to similar loadings as the intrapulmonary airways). We impose a drop in external pressure in the downstream half of the trachea as shown in Fig. 10. The effective plueral pressure during maximal effort is taken as the sum of maximal dynamic effort (Hyatt and Flath, 1966) and elastic recoil pressure. However, since the maximal dynamic effort depends on the flow rate (the result of the calculation) we use the maximal possible values given by Hyatt et al., (1966), as representative of the greatest potential influence of an external pressure gradient.

The loci of critical points for maximal lung volume (V_L=100% TLC) with uniform external pressure, and with a presumed gradient in external pressure are shown in Fig. 11. The differences are seen to be restricted to that region where the pressure gradient is non-zero. In Fig. 11 the open circles signify the FLS locations which satisfy the upstream boundary conditions. The results for maximal flow rate and the predicted flow limiting sites are given in Fig. 12. The flow rate is virtually unaffected by the pressure gradient at lower lung volumes when the FLS is located further upstream, away from the pressure gradient. The main observable effect of the pressure gradient is to displace the FLS upstream in those cases for which the FLS is found be in the zone of a significant gradient in external pressure. These results justify our earlier assumption of uniform external pressure. We note, however, that a reduction in external pressure acting on the extrathoracic airways might significantly alter their cross-sectional area even though the limiting flow rate is unchanged.

As noted earlier, the gradient of effective external pressure may negate the equivalence between a forced expiration and a forced evacuation.

The Competing Influences of Friction and Variations in Airway Stiffness

The process by which the transition point is reached is described in the section on the model. In essence, the numerator of the RHS of equations (16) and (17) must be positive for $S<1$, pass through zero when $S=1$, and be negative when $S>1$. The magnitude and sign of the numerator depends, in general, on a complex interaction between area change and variations in stiffness and friction. Since A_o is generally decreasing from $\xi=0$ to $\xi=1$, the contribution due to area change tends to drive the flow toward $S=1$, except in the trachea where the effect of area change is small. According to earlier assumptions, vessel stiffness monotonically increases. The corresponding term in the numerator of equation (16) and (17), as S approaches 1, is therefore negative, driving S away from unity. The friction term, which always retains the same sign, drives S toward unity in all cases. The dominant balance in this equation is between friction (driving S toward 1) and variations in stiffness (driving S away from 1). Consequently, for a given network geometry, the location of the FLS is primarily determined by the effects of friction and of variations in stiffness along the conducting system. Increasing the stiffness coefficient (C_k) or decreasing the friction coefficient (f_m) both drive the FLS upstream. Since at the FLS the Reynolds number is large (typically greater than 10^4), friction is dominated by the second of the two terms in equation (15). Therefore, high values for b drive the FLS downstream; and in fact, for b=0.0035 (the value obtained by Reynolds and used by Wilson and Lambert) there are no transition points within the conducting system and, instead, choking occurs at the downstream end ($\xi=1$). This is characterisitc of friction-dominated flows as discussed by Shapiro (1977).

For the values used in this study, (b=0.0013; C_k=2.40)the FLS is located in the trachea at large lung volumes and moves into the second generation at approximately 50% of TLC. Under no circumstances, in fact, with the specified parameters, does the FLS move further upstream than the second generation. With other specified distributions of rest area, tube wall properties and frictional behavior, however, this result too can vary. In the standard simulation the laminar friction behavior at the peripheral generation is such that the frictional dissipation is 1.5 (a in equation (15)) times as large as that in Poiseuille flow (Reynolds, 1982). The excess dissipation is presumably associated with the effects of branching and curvature. We found, however, that the results of the simulation are virtually independent of the values used for a; in doubling a to 3.0, we obtained results which are indistinguishable in Fig 5.

It is interesting to note that the maximal (critical) flow rate at a fixed lung volume is relatively independent of either

the frictional term or changes in the mechanical properties of the conducting system. This can be seen in Fig. 5a in which all the computed flow rates for a system with fixed geometry but with different friction and stiffness distributions are in a narrow band with deviations of less than 10%.

Physiological Limitation

The experimental data and the predicitons of the model presented in Figure 5(a) exhibit clear differences in maximal flow both at high and low lung volume. The differences at low lung volume have been discussed above in the context of the effects of gas viscosity and will be addressed again later. At high lung volume, the differences are caused by limitations imposed by the respiratory muscles as first demonstrated by Hyatt et al . In this case, the respiratory muscles are incapable of producing sufficient force to reach the point of wavespeed flow limitation. Instead, maximal flow is observed to be effort dependent.

To incorporate the effects of physiological limitation into the model, we used the data of Hyatt et al to predict the maximal effort associated with each lung volume. Their results can be plotted as in Figure 7 in terms of maximal presssure as a function of the rate at which the lung is emptying (related to the velocity of muscle contraction). The intersection of these curves with the maximal flow curve predicted by the model determines the true maximal flow at each lung volume. Those lung volumes for which the intersection occurs before the plateau in the flow curve is reached will exhibit effort dependent maximal flow. Our simulation predicts that this would occur at a lung volume of about 85% TLC as compared to a value of about 75% according to Mead et al. Note that if expiration is produced by applying progressively lower pressures at the mouth, then the point of wavespeed limitation will ultimately be attained, regardless of lung volume and muscular capability. Accordingly, the MEFV curves produced by forced evacuation will differ from those fo a forced expiration at high lung volumes, a difference which has been observed experimentally.

Effects of a Local Perturbation

In our previous work , we investigated the effects of applying a local perturbation in the distribution of airway stiffness, reference cross-sectional area, or external pressure. In those studies, we found that the flow can be driven toward a transition point by any of the following: (i) a local minimum in A_o, (ii) a local minimum in K_o, and (iii) a local maximum in the effective external pressure. In the presence of one of these factors, the transition to supercritical speed might occur at a more peripheral point in the lung when either normal or pathological variations in airway structure or geometry produce

any of the above conditions. Moreover, these points will continue to be preferential sites for flow limitation as lung volume decreases; then, rather than the smooth progress of the FLS toward the periphery predicted in the present calculations, the FLS might progress upstream at a non-uniform rate. With a sufficiently strong perturbation, the FLS might tend to jump to or from the region of the perturbation in a quasi-discontinuous fashion, producing an observable 'glitch' in the flow-volume curve.

Uncertainties in the Modeling Process

It is of interest to note that the model developed by LW was better able to simulate maximal flows and the effects of gas viscosity at low lung volumes than the model presented here. They accomplished this by adjusting their pressure-area relationships for the small airways until the predicted flow matched the flows obtained experimentally with air. In doing so, their small airways were made extremely compliant (e.g., their 16th generation airway undergoes a ten-fold increase in cross-sectional area as transpulmonary pressure increases from zero to 3 cmH_2O. In addition, the pressure-area law they used for negative transmural pressure (encompassing much of the airway system during a forced expiration, especially at low lung volumes) was based on an extrapolation from data obtained exclusively in the positive pressure range.

In the LW study, as in ours, the greatest weakness lies in the lack of reliable and appropriate experimental data on which to base the model. While the tube law used in our calculations is more closely related to actual experimental data, it was necessary to make several assumptions (most notably the variation in stiffness in the airway system) that are only weakly supported. Another potential deficiency, possibly related to the failure of our model at low lung volumes, concerns the friction law used in the calculations. This is essentially the same as that used by LW but with different values for the two constants. The method used to infer a local pressure drop relationship from measurements across an entire network may produce a misleading result for the following reason. Consider, for example, the behavior at the extremes of high and low Reynolds number. At sufficiently low Re, the flow should readily adjust at each junction. Consequently, the velocity profiles will be nearly parabolic, and the pressure drop will be very nearly that of Pouseuille flow (giving a=1.0). At high values of Re, energy dissipation due to turbulence will dominate and, even allowing for the loss of energy due to the generation of secondary flow, the pressure drop should be near that associated with a moderately rough pipe. Both estimates are considerably below the inferred values of Reynolds . The explanation for this apparent discrepancy may be associated with the flow behavior at

any of the above conditions. Moreover, these points will continue to be preferential sites for flow limitation as lung volume decreases; then, rather than the smooth progress of the FLS toward the periphery predicted in the present calculations, the FLS might progress upstream at a non-uniform rate. With a sufficiently strong perturbation, the FLS might tend to jump to or from the region of the perturbation in a quasi-discontinuous fashion, producing an observable 'glitch' in the flow-volume curve.

Uncertainties in the Modeling Process

It is of interest to note that the model developed by LW was better able to simulate maximal flows and the effects of gas viscosity at low lung volumes than the model presented here. They accomplished this by adjusting their pressure-area relationships for the small airways until the predicted flow matched the flows obtained experimentally with air. In doing so, their small airways were made extremely compliant (e.g., their 16th generation airway undergoes a ten-fold increase in cross-sectional area as transpulmonary pressure increases from zero to 3 cmH_2O. In addition, the pressure-area law they used for negative transmural pressure (encompassing much of the airway system during a forced expiration, especially at low lung volumes) was based on an extrapolation from data obtained exclusively in the positive pressure range.

In the LW study, as in ours, the greatest weakness lies in the lack of reliable and appropriate experimental data on which to base the model. While the tube law used in our calculations is more closely related to actual experimental data, it was necessary to make several assumptions (most notably the variation in stiffness in the airway system) that are only weakly supported. Another potential deficiency, possibly related to the failure of our model at low lung volumes, concerns the friction law used in the calculations. This is essentially the same as that used by LW but with different values for the two constants. The method used to infer a local pressure drop relationship from measurements across an entire network may produce a misleading result for the following reason. Consider, for example, the behavior at the extremes of high and low Reynolds number. At sufficiently low Re, the flow should readily adjust at each junction. Consequently, the velocity profiles will be nearly parabolic, and the pressure drop will be very nearly that of Pouseuille flow (giving a=1.0). At high values of Re, energy dissipation due to turbulence will dominate and, even allowing for the loss of energy due to the generation of secondary flow, the pressure drop should be near that associated with a moderately rough pipe. Both estimates are considerably below the inferred values of Reynolds . The explanation for this apparent discrepancy may be associated with the flow behavior at

intermediate Renolds numbers, in the range $10<Re<1000$, where the first term in equation (15) still dominates. Due to the combined effects of the induced secondary motion and the net reduction in flow area as seen by gas exiting from the lung, the velocity profiles will be quite blunt rather than parabolic. Hence the laminar coefficient in equation (15) should increase with increasing Re, rather than remain constant as it is forced to do in the current formulation. In forcing all the data to conform to the simple form of equation (15), the effects of an increase in viscous shear stress (an effective increase in a) is reflected instead by an increase in both a and b. Increasing b produces the correct overall pressure drop, but has the undesired effect of reducing the real effect of gas viscosity as predicted by the model.

A significant increase in a would tend to increase the influence of gas viscosity on maximal flows without the necessity of making the peripheral airways more compliant. However, to determine the ultimate validity of these arguments will require more definitive data both on the local pressure drop characteristics, and on the constitutive relations for the smaller airways.

Directions of Further Research

The model presented here represents one step toward developing a more realistic simulation of a forced expiration. We want to emphasize, though, the need for further investigations. In this initial study, we have identified several areas where additional research is needed before the models can be refined. These include: (1) the tube law, especially for the peripheral airways, (2) the expression used to describe the pressure drop due to frictional effects, (3) the behavior of supercritical flow and elastic jumps in pulmonary airways, and (4), the effects of asymmetry in the branching geometry and distribution of flow. The first two have been discussed previously. The third point arises from the recognition that nearly all studies of supercritical flow and elastic jumps have been conducted in latex rubber (penrose) tubes filled with water. It is entirely possible that the stability of such flows is different from that in the flow of gas through the conducting airways. The presence of instabilities could lead to solutions of a very different character downstream of the FLS from those predicted by the model since the latter presumes the existence and stability of a quasi-steady flow. And finally, it is essential that we recognize the potentially important implications of asymmetry . While it is gratifying to see the degree of agreement between this simple model and real flows, it is, at some time, surprising that a structure so complex yields to so simple an analysis. There is clearly much to be learned from the effects of lung asymmetry.

IV. PATIENT STUDIES

One of the outcomes of our modelling efforts was a better appreciation of how maximum expiratory flow could influence lung gas volume during HFV. In our progress report last year, we described experiments in which the mechanism of the hyperinflation observed during HFV was thought to be expiratory flow limitation. In this year we describe additional experiments designed to approach this hypothesis. In order to make appreciation of both sets of experiments simpler, we will include both sets of results in this year's progress report.

1. Introduction.

It has now been well established that dynamic hyperinflation of the lungs may occur in animals (Simon et al, 1984) or in patients (Reheder and Didier, 1984; Saari et al, 1984) during low tidal volume, high frequency oscillatory ventilation (HFOV). Simon et al (1984) originally attributed this phenomenon, which they observed in normal dogs, to asymmetry of pulmonary impedance during inspiration and expiration. We have noted, based on analysis of cineradiobronchographs (Gavriely et al, 1985), that asymmetric variations in airway diameter about the mean occur in canine central airways during HFOV. When this occurs, airway opening pressure tracings show similar asymmetry, with larger negative deflections than positive deflections from the mean. Similar airway opening pressure asymmetries have been observed in patients during HFOV.

These studies were undertaken in patients with respiratory failure to address the mechanisms responsible for dynamic hyperinflation and the associated airway opening pressure fluctuation asymmetry. To do so, we measured changes in lung volume during HFOV, and compared these results with steady maximum expiratory flow curves, as well as with predictions made by a series of computational models, each of which incorporated a different mechanism which could lead to dynamic hyperinflation. We found that expiratory flow limitation, rather than fixed asymmetric or variable asymmetric resistance, best accounted for our experimental observations.

2. Methods.

Patient Studies

Five female patients (ages 28-86) with chronic respiratory insufficiency served as subjects for the study. Each required long-term mechanical ventilatory support for underlying neuromuscular disease (patients #1-4) or for severe obstructive lung disease (patient #5). Informed consent for the protocol as institutionally approved was obtained from each patient. The patients tolerated applications of HFOV (see below) well, without apparent or stated discomfort.

Changes in lung volume were assessed with a Respitrace impedance plethysmograph. Belts were positioned around the abdomen and around the chest; relative gains were adjusted so that changes in the sum of the two signals were directly proportional to changes in mean lung volume. Calibration of the Respitrace volume signal was performed by delivering a number of increments of gas from a calibrated syringe into the patient. The measured volume signal was linear over the range of volumes studied; the calibration was unaffected by applied oscillation as demonstrated previously (Saari et al, 1984). Each patient was studied in the supine position and did not change posture or body position during the study.

Two series of experiments were performed. In Series A, the dependence of lung volume on HFOV frequency and mean airway opening pressure was determined in three subjects. In Series B, we compared maximal expiratory flow curves with the peak expiratory flow vs. lung volume relationship found during HFOV in four subjects.

Series A

The high frequency oscillatory ventilator included a sealed piston oscillator and a high impedance bias flow (Rossing et al, 1984). Air or an air-oxygen mixture was bled into the system from a high pressure source across a needle valve. The bias outflow (rate 16-20 L/min, measured with a calibrated rotameter) was servo-controlled to maintain mean airway opening pressure at a predetermined level (2-13 cm H_2O) with a 3 second time constant, independent of whether or not oscillations were applied. Airway opening pressure (Pao) was measured through a lateral side arm at right angles to the 13 mm i.d. HFOV delivery tube, using a solid state pressure transducer (Ailtech MS-10); mean airway opening pressure was obtained electronically. Fifty or 100 ml sinusoidal oscillations (frequency 0.5-20 Hz) were provided by the sealed piston pump driven by a linear magnetic motor. Tidal volume was measured by integrating airway flow (measured with a number 2 Fleisch pneumotachograph and a Validyne MP-45 $\pm$ 50 cm H_2O pressure transducer) placed between the bias flow inlet and the airway opening. To calibrate the tidal volume signal, we used the HFOV apparatus to deliver tidal volumes into and out of a large rigid vessel of known adiabatic compliance. Integrated flow was related to delivered tidal volume (derived from pressure changes in the rigid vessel) at each frequency-tidal volume combination to be employed.

The patient's tracheostomy tube was disconnected from the conventional ventilator and the patient allowed to exhale to FRC (Pao=0 cm H_2O) for 5-10 seconds, until the patient's lung volume, as measured by the Respitrace, was stable. The subject was then connected to the HFOV apparatus with the oscillator turned off, at which time the lungs were inflated by the bias flow circuit until a new stable lung volume, determined by the prechosen mean Pao, was reached. Sinusoidal oscillations were applied at a prechosen frequency and tidal volume for 30-45 seconds; further changes in lung volume were monitored by the impedance plethysmograph, and the subject was then returned to the conventional ventilator. The entire sequence was repeated as HFOV frequency and tidal volume and mean airway opening pressure were systematically varied.

Series B

Maximal expiratory flow-volume curves were generated as follows. Each subject was allowed to relax to FRC; the patient's tracheostomy cannula was then connected to a 3 liter syringe. 1500 ml were delivered from the syringe into the patient; 2 seconds later, the syringe plunger was rapidly and forcibly withdrawn, effecting a maximal expiration. Two to five such maximal expirations were performed over a 10-15 minute period. Lung volume versus time curves during these maneuvers (obtained from impedance plethysmograph tracings) were averaged as volume as a function of time, and a maximum expiratory flow-volume curve was obtained by discrete differentiation of the average volume-time curve every 0.1 sec.

After completion of the above maneuvers, the HFOV piston pump used in Series A was used to deliver sinusoidal oscillations of volume 50 to 400 ml at frequencies between 0.33 and 10 Hz. The bias flow apparatus was replaced by an oxygen-filled weighted spirometer, which supplied gas through a high impedance to oscillatory flow (Saari et al, 1984) such that mean airway opening pressure was maintained at 2-3.5 cm H_2O. Periods of HFOV were applied as in Series A until a new stable lung volume was reached, several HFOV frequency-tidal volume combinations were applied in sequence without return to FRC or

mechanical ventilation, but never for more than 60 seconds without returning to conventional ventilation. Changes in lung volume were recorded using the impedance plethysmograph.

Computational Model

Three electrical circuits (Figure 13) were used to model the mechanical behavior of the high frequency ventilator and the respiratory system. In the analogy, current was used to model volume flow, and voltage was used to reflect pressure (atmospheric pressure was considered as ground potential). The HFOV pump was thus a current source (Ipump); the bias flow was modelled with a voltage source (Vmap), whose value represented mean airway pressure, coupled to the airway opening node by a large inductance (Lbf). This configuration resulted in a high impedance to oscillatory flow (Butler et al, 1980). The respiratory tree was modelled as a central airway "shunt" compliance (Caw), which reflects potential radial oscillatory motion of central airway walls, and the remaining lung as a path from the airway opening node to the alveolar volume, modelled as a pure compliance (Calv). Inspiratory and expiratory limbs of the latter path were isolated by diodes to facilitate implementation of asymmetry (Simon et al, 1984).

The inspiratory limb in all three models consisted of a fixed inspiratory resistance (Rinsp) leading to the alveolar node. The structure of the expiratory limb was varied to model each of three types of asymmetric airways impedance. Fixed asymmetric resistance (Figure 1a) was modelled using a linear resistor (Rexp); variable asymmetric resistance (Figure 1b) was modelled with a variable resistance whose value varied inversely with lung volume [Rexp(Palv)]; and expiratory flow limitation (Figure 1c) was modelled using a PNP transistor to limit flow (current) in series with a resistance (Rexp) whose value was equal to that of Rinsp. The transistor collector-emitter voltage-current characteristic (Gray et al, 1969) was chosen to mimic the isovolume pressure-flow relationships of human lungs (Hyatt et al, 1958). The maximum allowable expiratory flow through the transistor is determined by Palv and Vcrit. Vcrit represent the value of Palv at which there is no allowable expiratory flow. As Palv (and lung volume) rises above Vcrit, the maximum allowable expiratory flow rises proportionally to the difference between Palv and Vcrit. Component values were chosen to reflect physiologic parameters typical of patients such as those in our study, and are listed for each model in Table 1. Tidal volume was set to 100 ml; frequencies of 1 to 8 Hz were used. Mean airway pressures of 3 and 10 cm H_2O were studied for each type of asymmetry.

Simulations of HFOV by these models were performed by an iterative integration computer program (SPICE2, copyright Univ. of Calif., Berkeley) for a sufficiently long interval to attain a steady state. Excursion extremes of Palv and Pao were taken from the last second of simulation, and mean Palv was estimated as the average of excursion extremes.

3. Results.

Patient Studies

Series A

The dependence of dynamic hyperinflation on frequency and on mean airway

opening pressure is illustrated in Figure 14. When mean airway opening pressure was low (2-5 cm H_2O), dynamic hyperinflation occurred during HFOV at relatively low frequencies, and lung volume increased with frequency such that over a one liter dynamic change in FRC was observed in 2 subjects. In contrast, when the mean airway pressure was raised (7-13 cm H_2O), a different dependence of dynamic hyperinflation on frequency was observed at the same V_T. The elevated mean airway opening pressure was associated with an elevated mean lung volume over resting FRC before oscillations were applied, and there was no further increase in lung volume as frequency was raised, until the frequency reached some critical value (approximately 2-4 Hz). Above this critical frequency, lung volume increased with frequency in a fashion nearly parallel to that observed at the lower mean airway opening pressure[1]. As demonstrated previously, the degree of dynamic hyperinflation was greater at each frequency when larger tidal volumes were applied at constant mean airway opening pressure (Figure 15).

To define the importance of expiratory flow rate in dynamic hyperinflation during HFOV, we varied the inspiratory-expiratory duration (I:E) ratio of the oscillation from 1:2 to 2:1 in two subjects, during HFOV with fixed V_T (100 ml) and mean Pao (2 cm H_2O). A quasi-sinusoidal volume waveform was used. Dynamic hyperinflation was most pronounced at any frequency when the greatest I:E ratio was applied. These data are expressed as a function of mean expiratory flow in Figure 16.

Series B

Figure 17 presents expiratory flow versus lung volume relationships found during steady forced maximal expiratory flow and during HFOV applications. HFOV data are expressed as peak expiratory flow at the airway opening versus lung volume. The peak expiratory flow during HFOV was almost always greater than that found during the steady forced maximal expiration maneuver at the same lung volume. Subject #1, who demonstrated the least difference between oscillatory and steady expiratory flow-volume relationships, demonstrated the least impaired steady maximal expiratory flow-volume curve. In addition, she was the youngest patient, and clinically had the least severe functional pulmonary impairment, as judged by usual arterial blood gases, frequency of respiratory infections, and chronic inspired oxygen fraction requirement.

Model Predictions

The dependence of lung volume on frequency and mean airway opening pressure predicted by each of the three asymmetric respiratory impedance models is illustrated in Figure 18. In the first model, the expiratory limb of the respiratory path was composed of a fixed resistance whose magnitude was twice that of the inspiratory resistance. At low mean Pao (3 cm H_2O), lung volume progressively increased with frequency throughout the range of frequencies simulated. Raising mean Pao to 10 cm H_2O raised lung volume but had no effect on the shape of the lung volume - frequency relationship. There was no range of frequencies over which lung volume was independent of frequency at either mean Pao. The second model incorporated an expiratory resistance whose magnitude varied inversely with lung volume. At low mean Pao, there was a more rapid rise of lung volume with frequency than was seen in the fixed asymmetry model, reflecting the greater degree of impedance asymmetry at low lung volumes

(Table 1); however, the dependence of lung volume change on frequency was otherwise similar to that found for the case of fixed asymmetry. At high mean Pao, the variable Rexp model predicted somewhat less dynamic hyperinflation at the higher frequencies than did the fixed asymmetry model, reflecting the smaller degree of asymmetry at high lung volumes (Table 1), but there was still a progressive rise of lung volume with frequency. Thus, predictions of both the fixed and variable expiratory resistance models are qualitatively different from the dependence of lung volume on HFOV frequency and mean Pao observed in our Series A patients, in that neither demonstrates a plateau of lung volume over a range of low frequencies.

In contrast, the dependence of lung volume on frequency and mean Pao predicted in the expiratory flow limitation model did qualitatively resemble that observed in our patients. A monotonic increase in lung volume with frequency was evident at low mean Pao; when mean Pao was raised, a plateau of lung volume over a range of lower frequencies appeared.

While the dependence of the lung volume - frequency relationship on mean Pao varied substantially among the three models, several features of the models' predictions were strikingly similar. First, all three models predicted airway opening pressure fluctuations with qualitatively similar asymmetries about their means; further, the diminution of fluctuation asymmetry with time recently reported by Rehder and Didier (1984) occurred with all three modes of impedance asymmetry. Second, the time delay between excursions of airway opening (Pao) and alveolar pressures (Palv) in each model is about one-quarter cycle, with Pao leading Palv (Figure 19). Since Pao and Palv are each proportional to the tidal volumes delivered to the central airway shunt compliance and alveolar zones, respectively, these two parts of the tidal volume introduced into the trachea must also be out of phase. Thus, the sum of the "shunted" and "peripheral" portions of tracheal tidal volume is greater than the tidal volume introduced into the trachea itself. Figures 20a and 20b show that the magnitude of shunted and peripheral tidal volumes are closely similar for each of the three models of asymmetric lung impedance; substantial "shunt" airway tidal volumes are evident at the higher frequencies in each case. Dependence of oscillatory flow delivered to the alveoli on frequency and mean Pao, shown in Figure 21, is nearly identical among the three models of lung asymmetry. Distal oscillatory flow increased roughly linearly with frequency at low frequencies, then rose less rapidly with higher frequencies above a critical frequency, about 4 Hz. In addition, oscillatory flow in the alveolar zone depended little on mean Pao.

4. Discussion.

Dynamic pulmonary hyperinflation has been shown to occur during high frequency, low tidal volume oscillatory ventilation (HFOV) in both animals and man. Various investigators have suggested that this phenomenon stems from differing inspiratory and expiratory impedances to airflow. Such differences could arise from the asymmetries in resistive pressure dissipation that are known to occur between inspiration and expiration in a rigid branching network (Reynolds and Lee, 1981). Lung volume dependence of resistance (Mead and Whittenberger, 1956) could also contribute to dynamic hyperinflation, and dynamic narrowing of the airways reflecting expiratory flow limitation is a third possible mechanism contributing to dynamic hyperinflation. We thought

that it might be possible to distinguish among these mechanisms by modelling the electrical analog of each and comparing general aspects of predictions made from each model to data sets obtained in patients demonstrating hyperinflation during HFOV. Our data are compatible with the hypothesis that hyperinflation arises as a result of expiratory flow limitation.

Our models utilized both well established and novel electrical analogs to simulate various aspects of the mechanical behavior of the respiratory system. All three models incorporated a shunt capacitor (Caw) to model central airway compliance, as suggested by Mead (1969). During an oscillatory cycle, this capacitor receives a fraction of the tidal volume delivered at the airway opening, and this fraction varies with the oscillatory frequency. Although up to 70% of the airway opening tidal volume was delivered onto the airway shunt capacitor (at high frequency), this volume was then exhaled into the alveolar zone compliance. Thus, to the extent that our models predict real lung behavior, central airway shunting might decrease HFOV efficiency somewhat by absorbing a fraction of the tidal volume delivered at the airway opening (Rossing et al., 1981). However, this mechanism might also serve to enhance mixing between the central airways and the alveolar zone.

A number of novel features were incorporated into our electrical analogs. First, we isolated the inspiratory and expiratory limbs of the model using idealized diodes, as suggested recently by Simon and coworkers (1984). This allowed independent manipulation of the expiratory limb without alteration of the inspiratory limb or the rest of the model. Second, we simulated the role of the bias flow in maintaining constant mean airway opening pressure by using a voltage (pressure) source connected to the airway opening by a large inductance. Since the impedance of this inductor increases with frequency, it excludes oscillatory flow while allowing steady mean airway opening pressure to be maintained, after an initial transient. Note that, as during HFOV, the bias flow pressure source provides the volume which enters the lung during hyperinflation; it is the only source of volume (charge) in these models. Third, we have employed a bipolar transistor as a lumped parameter model of expiratory flow limitation. In the configuration used, the transistor allows flow through its axial path of magnitude less than or equal to a maximum value. This maximum flow limit is proportional to the pressure difference between Palv and Vcrit (the critical airway closing pressure), and is independent of the downstream pressure, provided that the downstream pressure is sufficiently low to cause flow limitation to occur. The only way to increase maximum flow in the expiratory limb is for Palv to increase.

Similar mechanisms also account for dynamic hyperinflation in the other two models; differences stem only from the determinants of the degree of asymmetry in each model. In the model with lung volume dependence of expiratory resistance, the relationships between Palv and frequency for the two values of mean airway opening pressure examined were not parallel; this results because Rexp is lower at all values of frequency for the higher mean Pao, and the incremental decrease in Rexp for unit changes in lung volume are less at higher lung volumes. Clearly, the precise relationships obtained between Palv (lung volume) and frequency at various values of mean Pao in this model will depend on the relationship chosen for Rexp as a function of Palv. We chose an inverse relationship for this model based on the data Dubois and co-workers (1956) obtained during panting. Of course, during external forced oscillation

at these tidal volumes and frequencies, other relationships may apply. Nevertheless, both models which do not incorporate dynamic flow limitation predict a dependence of Palv on frequency at various mean airway pressures substantially different from that which we observed experimentally. Thus, it seems likely that these two models fail to incorporate vital features of the mechanical behavior of our patients' respiratory systems.

In contrast, our model which incorporated dynamic flow limitation demonstrated a dependence of Palv on frequency which was quite similar to that observed in all three of the subjects we studied. The critical feature which was uniquely similar in both the data and the flow limitation model was the relationship between Palv and frequency at low frequencies (less than 2-3 Hz) at high and low mean airway opening pressures. This results from the fact that the maximum expiratory flow allowed through the transistor depends only on lung volume. With high mean Pao, the elevated lung volume allows a maximum expiratory flow which is greater than that required at low frequencies. In this circumstance, there is no flow limitation, and the transistor appears as a short-circuit, with no resistance. Thus, at frequencies below the critical frequency (3 Hz for mean Pao = 10 cm H_2O and V_T = 100 ml), there is no symmetry of inspiratory and expiratory paths, and no dynamic hyperinflation occurs. In contrast, with lower mean Pao (and lower initial lung volume), the expiratory flow required even at lower frequencies may exceed that allowed at the lower lung volume.

In this flow limitation model, we used transistor characteristics which reflect features of isovolume pressure-flow curves obtained during steady flow. We realize that these relationships may not prevail during oscillatory flow, and therefore compared the expiratory flow-volume relationships during HFOV to those during forced maximal exhalations in Series B. Our results clearly demonstrate that oscillatory and steady expiratory flow-volume relationships need not be the same, a result considered in more detail below. Nevertheless, the similarity of the model's predictions and our experimental observations provides support for the hypothesis that expiratory flow limitation accounts in large part for the dynamic hyperinflation observed during HFOV.

Further support for the hypothesis that dynamic hyperinflation results from expiratory flow limitation can be gathered from Figure 16. By varying inspiration-expiration duration ratio (I:E), we varied mean expiratory flow while maintaining tidal volume, frequency, and mean airway opening pressure constant. Though I:E ratio substantially influenced lung volume change for fixed frequency, tidal volume, and mean airway opening pressure, its had little influence when change in lung volume was considered as a function of mean expiratory flow. This result indicates that changes in I:E ratio influenced the degree of dynamic hyperinflation simply by changing expiratory flow, which likely determines the degree of dynamic hyperinflation.

In Series B, we directly compared the lung volumes needed to sustain expiratory flows during HFOV with the flow-volume relationship observed during a steady forced maximal expiration (MEFV) from 1.5 L above FRC. At any lung volume, peak expiratory flow during HFOV exceeded that during the MEFV maneuver by several-fold. A number of phenomena can result in expiratory flow at a given lung volume greater than that observed during a steady forced maximal expiration. First, dynamic collapse of central airways can lead to

augmentation of expiratory flow at the onset of forced expiration (Knudson et al., 1974). This occurs only once during a MEFV maneuver but, during HFOV, could occur with every cycle. Such repeated airway collapse would result in far greater peak expiratory flow at the trachea than out of the alveoli; the MEFV curve, though, is vastly more dependent on the latter. Second, the distribution of oscillatory flow may be different, at any lung volume, from that of maximal expiratory flow. For example, during a partial forced expiratory flow maneuver (Melissinos et al., 1979), initial flow favors lung regions with short time constants; it may be that flow during HFOV originates from the "faster" expiratory pathways of a non-homogeneous lung. Indeed, in patients with obstructive lung disease, the expiratory flow during a partial forced expiration may exceed that during a MEFV maneuver from TLC by over 2 times (Takishima, et al., 1967). Note that in each of the cases above, the mechanism leading to dynamic hyperinflation is still expiratory flow limitation, even though a different expiratory flow versus lung volume characteristic may determine the degree of dynamic hyperinflation.

In summary, through the combined use of electrical analog modelling and experimental observations in intubated ventilator-dependent patients, we propose that expiratory flow limitation is responsible for the impedance asymmetry that leads to dynamic pulmonary hyperinflation during HFOV. The expiratory flow-volume relationship which leads to this asymmetry during oscillatory flow may differ substantially from that which prevails during steady forced maximal expiration. This difference stems from an as yet uncertain mechanism, but may provide insight into the time course of dynamic airway narrowing or into the distribution of oscillatory flow when it is further studied.

REFERENCES

1. Butler, W.J., D.J. Bohn, A.C. Bryan, and A.B. Froese. Ventilation by high frequency oscillation in humans. Anesth. Analg. (Cleve) 59:577-84, 1980.

2. Clement, J., J. Pardaens, and W. van de Woestijne. Expiratory flow-rate, driving pressures, and time-dependent factors. Simulation by means of a model. Resp. Physiol. 20:353-369, 1974.

3. Clement, J., W. van de Woestijne, and J. Pardaens. A general theory of respiratory mechanics applied to forced expiration. Respiratory Physiology. 19:60-79, 1973.

4. Cowley, S.J. Elastic jumps on fluid-filled elastic tubes. J. Fluid Mechanics. 116:459-473, 1982.

5. Dubois, A.B., S.Y. Botelho, and J.H. Comroe, Jr. A new method for measuring airway resistance in man using a body plethysmograph: Values in normal subjects and in patients with respiratory disease. J. Clin. Invest. 35:327, 1956.

6. Elad, D., R.D. Kamm, and A.H. Shapiro. Choking phenomena in a lung-like model. (submitted to Transactions of the ASME, J. Biomechanical Engineering). 1985b.

7. Elad, D., R.D. Kamm, and A.H. Shapiro. Model simulation of forced expiration, Part I: Semi-empirical tube law for bronchial airways. (submitted to Transactions of the ASME, J. Biomechanical Engineering). 1985a.

8. Gavriely, N., J. Solway, J.M. Drazen, A.S. Slutsky, R. Brown, S. Loring, and R.H. Ingram, Jr. Radiographic visualization of airway wall movement during oscillatory flow in dogs. J. Appl. Physiol. 58:645-652, 1985.

9. Gavriely, N., J. Solway, S.H. Loring, J.P. Butler, A.S. Slutsky, and J.M. Drazen. Pressure-flow relationships of endotracheal tubes during high-frequency ventilation. J. Appl. Physiol. 59:3-11, 1985.

10. Gray, P.E. and C.L. Searle. Electronic Principles: Physics, Models, and Circuits. John Wiley and Sons, Inc., New York. Chapter 7. 1969.

11. Green, M., J. Mead, and J.M. Turner. Variability of maximum expiratory flow-volume curves. J. Appl. Physiol. 37:67-74, 1974.

12. Hughes, J.M.B., F.G. Hoppin, and J. Mead. Effects of lung inflation on bronchial length and diameter in excised lungs. J. Appl. Physiol. 32:25-35, 1972.

13. Hyatt, R.E. Expiratory flow limitation. J. Appl. Physiol. 55:1-8, 1983.

14. Hyatt, R.E., and R.E. Flath. Influence of lung parenchyma on pressure-diameter behavior of dog bronchi. J. Appl. Physiol. 21:1448-1452, 1966.

15. Hyatt, R.E., and R.E. Flath. Relationship of air flow to pressure during maximal respiratory effort in man. J. Appl. Physiol. 21:477-482, 1966.

16. Hyatt, R.E., D.P. Schilder, and D.L. Fry. Relationship between maximum expiratory flow and degree of lung inflation. J. Appl. Physiol. 13:331-336, 1958.

17. Hyatt, R.E. and Wilcox, R.E. Extrathoracic airway resistance in man. J. Appl. Physiol. 16:326-330, 1961.

18. Hyatt, R.E., T.A. Wilson, and E. Bar-Yishay. Prediction of maximal flow in excised human lungs. J. Appl. Physiol. 48:991-998, 1980.

19. Jaeger, M.J. and H. Matthys. The pattern of flow in the upper human airways. Resp. Physiol. 6:113-127, 1967.

20. Klingele, T.G. and N.C. Staub. Terminal bronchiole diameter changes with volume in isolated, air-filled lobes of cut lungs. J. Appl. Physiol. 30:224-227, 1974.

21. Knudson, R.J., J. Mead, and D.E. Knudson. Contribution of airway collapse to supramaximal expiratory flows. J. Appl. Physiol. 36:653-667, 1974.

22. Lambert, R.K., T.A. Wilson, R.E. Hyatt, and J.R. Rodarte. A computational model for expiratory flow. J. Appl. Physiol. 52:44-56, 1982.

23. Macklem P.T. and D.F. Proctor. Factors determining maximum expiratory flow in dogs. J. Appl. Physiol. 25:159-169, 1968.

24. Martin, H.B. and D.F. Proctor. Pressure-volume measurements on dog bronchi. J. Appl. Physiol. 13:337-343, 1958.

25. Mead, J. Contribution of compliance of airways to frequency-dependent behavior of lungs. J. Appl. Physiol. 26:670-673, 1969.

26. Mead, J., P.T. Turner, P.T. Macklem and J.B. Little. Significance of the relation between lung recoil and maximum expiratory flow. J. Appl. Physiol. 22:95-108, 1967.

27. Mead, J. and J.L. Whittenberger. Physical properties of human lungs measured during spontaneous respiration. J. Appl. Physiol. 5:779-796, 1953.

28. Melissinos, C.G., P. Webster, Y.K. Tien, and J. Mead. Time dependence of maximum flow as an index of non-uniform emptying. J. Appl. Physiol. 47:1043-1050, 1979.

29. Mink, S., M. Ziesman, and L.D.H. Wood. Mechanisms of increased maximum expiratory flow during HeO_2 breathing in dogs. J. Appl. Physiol. 47:490-502, 1979.

30. Oates. G.C. Fluid flow in soft walled Tubes. I: Steady flow. Med. Biol. Eng. 13:773-778, 1975.

31. Pardaens, K.P., W. van de Woestijne, and J. Clement. A physical model of expiration. J. Appl. Physiol. 33:479-490, 1972.

32. Pedersen, D.F., B. Thiessen, and S. Lyager. Airway compliance and flow limitation during forced expiration in dogs. J. Appl. Physiol. 52:357-369, 1982.

33. Rehder, K. and E.P. Didier. Gas transport and pulmonary perfusion during high-frequency ventilation in humans. J. Appl. Physiol.: Respirat. Environ. Exercise Physiol. 57:1231-1237, 1984.

34. Reynolds, D.B. Steady expiratory flow-pressure relationship in a model of the human bronchial tree. Transactions of the ASME, J. Biomechanical Engineering. 104:153-158, 1982.

35. Reynolds, D.B. and J.S. Lee. Steady pressure-flow relationship of a model of the canine bronchial tree. J. Appl. Physiol.: Respirat. Environ. Exercise Physiol. 51:1072-1079, 1981.

36. Rossing, T.H., A.S. Slutsky, J.L. Lehr, P.A. Drinker, R. Kamm, and J.M. Drazen. Tidal volume and frequency dependence of carbon dioxide elimination by high-frequency ventilation. N. Engl. J. Med. 305:1375-1379, 1981.

37. Rossing, T.H., J. Solway, A.F. Saari, N. Gavriely, A.S. Slutsky, J.L. Lehr, and J.M. Drazen. Influence of the endotracheal tube on CO_2 transport during high frequency ventilation. Am. Rev. Resp. Dis. 129:54-57, 1984.

38. Saari, A.F., T.H. Rossing, J. Solway, and J.M. Drazen. Lung inflation during high frequency ventilation. Am. Rev. Resp. Dis. 129:333-336, 1984.

39. Shapiro, A.H. Steady flow in collapsible tubes. Transactions of the ASME, J. Biomechanical Engineering. 99:126-147, 1977.

40. Simon, B.A., G.G. Weinmann, and W. Mitzner. Mean airway pressure and alveolar pressure during high-frequency ventilation. J. Appl. Physiol.: Resp. Environ. Exercise Physiol. 57:1069-78, 1984.

41. Smaldone, G.C. and E.H. Bergofsky. Delineation of Flow Limiting Segment and Predicted Airway Resistance by Movable Catheter. J. Appl. Physiol. 40:943-952, 1976.

42. Solway, J., J. Fredberg, and J.M. Drazen. Lumped parameter model of the lung during maximal expiratory flow. Am. Rev. Resp. Dis., 1985. (in press) (Abstract)

43. Staats, B.A., T.A. Wilson, S.J. Lai-Fook, J.R. Rodarte, and R.E. Hyatt. Viscosity and density dependence during maximal flow in man. J. Appl. Physiol. 48:313-319, 1980.

44. Stanescu, D.C., J. Pattijn, J. Clement, and van de Woestijne. Glottis opening and airway resistance. J. Appl. Physiol. 32:460-466, 1972.

45. Takishima, T., G. Grimby, W. Graham, R. Knudson, P.T. Macklem, and J. Mead. Flow-volume curves during quiet breathing, maximum voluntary ventilation, and forced vital capacities in patients with obstructive lung disease. Scand. J. Resp. Dis. 48:384-393, 1967.

46. Takishima, T., H. Sasaki, and T. Sasaki. Influence of lung parenchyma on collapsibility of dog bronchi. J. Appl. Physiol. 38:875-881, 1975.

47. Weibel, E.R. Morphology of Human Lung. Academic Press, New York. 1963.

48. Wood, L.D.H., L.A. Engel, P. Griffin, P. Despas, and P.T. Macklem. Effect of gas physical properties and flow on lower pulmonary resistance. J. Appl. Physiol. 41:234-244, 1976.

TABLE 1

Component Values Incorporated into HFOV Models

Values common to all 3 models

Rinsp 20 cm $H_2O \cdot sec/liter$

Calv 0.05liter/cm H_2O
Caw 0.0008liter/cm H_2O

Lbf 25 cm $H_2O \cdot sec^2/liter$

Values pertinent to individual models

Fixed asymmetric resistance model
Rexp 40 cm H_2O/liter

Variable asymmetric resistance model

Rexp(Palv) 400/Palv cm H_2O sec/liter (when Palv is expressed in cm H_2O)

Flow limitation model

Vcrit 0 cm H_2O

Rflowlim $1.25*10^4$ cm $H_2O \cdot sec/liter$

PNP transistor forward beta 1000

These parameters result in a maximum expiratory flow rate equal to Palv*.08 liter/sec (when Palv is expressed in cm H_2O)

FIGURE LEGENDS

Figure 1. A schematic representation of the lung model used in these calculations.

Figure 2. Left: Distribution of cross-sectional area as a function of distance from the upstream (ξ=0) to downstream (ξ=1) end. Right: Distribution of number of airways located a distance ξ from the upstream end of the airway system.

Figure 3. The dependence of the loss coefficient C_d on Reynolds number.

Figure 4. (a) The locus of points, at each of several different lung volumes, at which a transition from S<1 to S>1 can be achieved. These curves are obtained by setting the numerator of equations (16) and (17) to zero with S=1. (b) A schematic representation showing how an elastic jump is 'fit' into the solution for Speed index as a function of distance. See text for complete description.

Figure 5. (a) Dimensional flow rate as a function of lung volume for several different combinations of the parameters of the model. Also shown are several sets of experimental data obtained on humans and dogs. (b) The location of the transition point (FLS) corresponding to the cases shown in (a). In all cases, the transition point moves upstream as lung volume decreases.

Figure 6. Plots of (a) area ratio, (b) speed index, (c) bronchial pressure minus alveolar pressure, and (d) bronchial pressure minus atmospheric pressure, showing the distributions with distance for several different levels of respiratory effort.

Figure 7. A collection of iso-volume-pressure-flow curves for different lung volumes generated by the model. Also shown are the respiratory limits (due to muscular limitations) as measured by Hyatt et al (1966).

Figure 8. (a) Dimensional flow rate as a function of lung volume for several different gas mixtures. (b) The location of the FLS corresponding to the cases shown in (a).

Figure 9. The level of driving pressure (plueral pressure) required to attain choked flow, plotted as a function of lung volume, for each of the three gas combinations shown in Figure 8.

Figure 10. The distribution of external pressure introduced to the model to simulate the effect of a reduction in external pressure for extra-thoracic airways.

Figure 11. The effect of the external pressure distribution shown in Figure 10 on the locus of transition points predicted by the model.

Figure 12. The effect of non-uniform external pressure (Figure 10) on maximal flow rate (a) and the location of the FLS (b).

Figure 13. Three electrical circuits used to model the mechanical behavior of the respiratory system during HFOV. Circuits are all similar except for the expiratory pathways, enclosed by the interrupted line. (a) Fixed asymmetric resistance; (b) Variable asymmetric resistance; (c) Expiratory flow limitation. See text for model descriptions; component values are provided in Table 1.

Figure 14. Dependence of dynamic hyperinflation during HFOV on frequency and mean airway opening pressure (mean Pao) in three patients. Ordinate is change of lung volume above FRC with mean airway opening pressure equal to atmosphere. Circles with broken lines denote higher mean Pao; stars with solid lines denote lower mean Pao.

Subject #	1	2	3
Higher mean Pao (cm H_2O)	9	8	13
Lower mean Pao (cm H_2O)	4	3	3

Figure 15. Dependence of dynamic hyperinflation during HFOV on tidal volume and oscillatory frequency at constant mean airway opening pressure in two patients. Ordinate is change of lung volume above FRC with mean airway opening pressure equal to atmosphere. Circles with broken lines denote tidal volume 100 ml; stars with solid lines denote tidal volume 50 ml.

Figure 16. Dependence of dynamic hyperinflation during HFOV on inspiration-expiration duration ratio (I:E) at constant tidal volume (100 ml) and 11/26/85way opening pressure, from 2 Series A patients. Dat

Figure 17. Expiratory flow versus lung volume relationships found in Series B patients. The solid line represents forced maximal expiration from 1.5 L above resting FRC; the data points shown are peak expiratory oscillatory flow obtained during HFOV.

Figure 18. Predicted dynamic hyperinflation during HFOV from each of three models of asymmetric lung impedance. (a) Fixed asymmetric resistance; (b) Variable asymmetric resistance; (c) Expiratory flow limitation. Circles with broken lines denote mean Pao 10 cm H_2O; stars with solid lines denote mean Pao 3 cm H_2O.

Figure 19. Lissajous figures displaying predicted alveolar pressure (Palv) versus predicted airway opening pressure (Pao) for each of three models of asymmetric lung impedance. (a) Fixed asymmetric resistance; (b) Variable asymmetric resistance; (c) Expiratory flow limitation. In each case, Pao leads Palv by about one quarter cycle; frequency was 4 Hz.

Figure 20. Predicted distributions of tidal volume entering the airway opening for each of the three models. (A) Central airway "shunt" volume (V_{Talv}); (a) Fixed asymmetric resistance; (b) Variable asymmetric resistance; (c) Expiratory flow limitation. Circles with broken lines denote mean Pao 10 cm H_2O; stars with solid lines denote mean Pao 3 cm H_2O.

Figure 21. Predicted dependence of distally delivered oscillatory flow ($F \times V_{Talv}$) during HFOV. (a) Fixed asymmetric resistance; (b) Variable asymmetric resistance; (c) Expiratory flow limitation. Circles with broken lines denote mean Pao 10 cm H_2O; stars with solid lines denote mean Pao 3 cm H_2O.

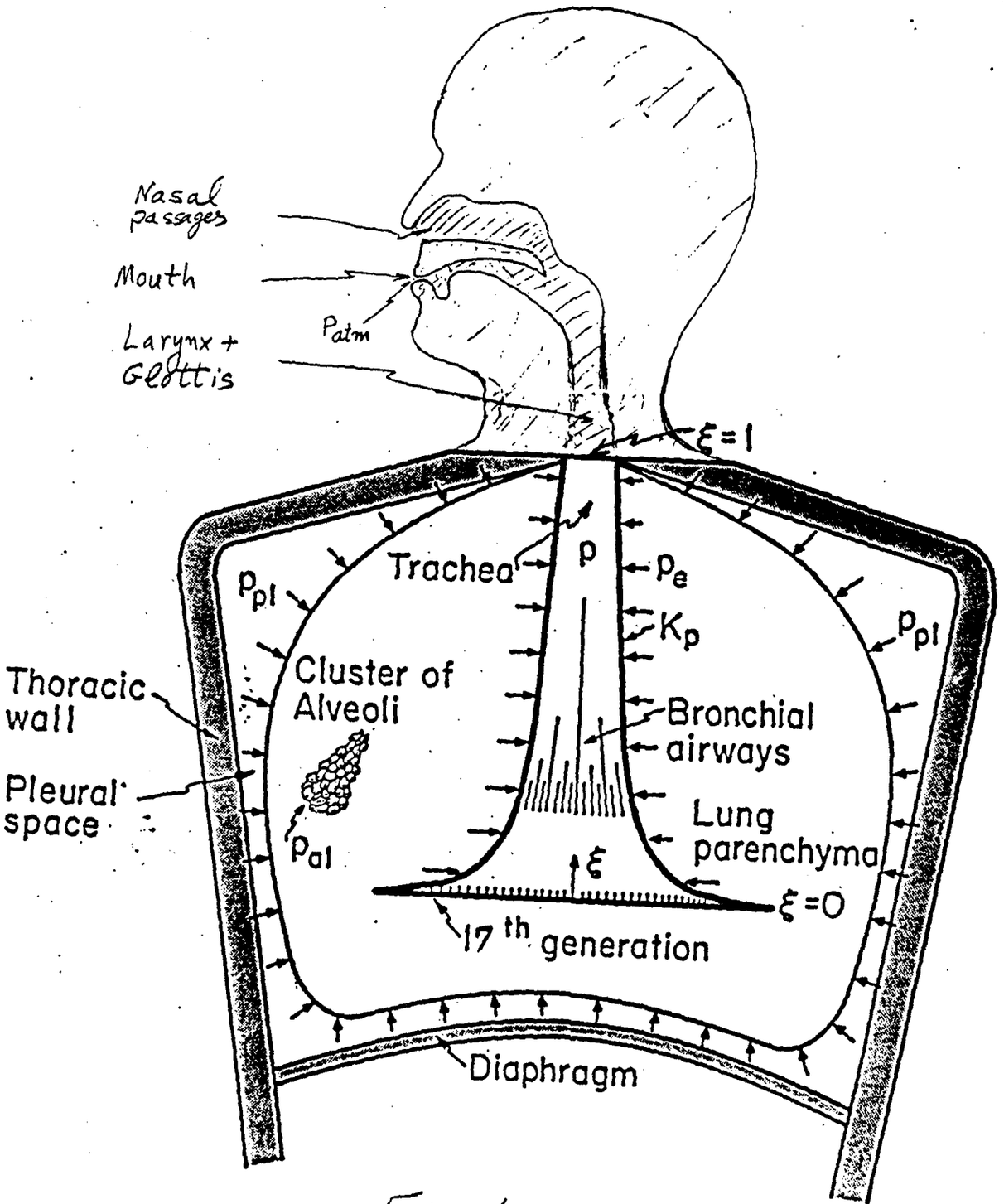
Nasal passages
Mouth
Larynx + Glottis
P_{atm}
$\xi = 1$
Trachea
p
p_e
K_p
p_{pl}
p_{pl}
Thoracic wall
Cluster of Alveoli
Bronchial airways
Pleural space
p_{al}
ξ
Lung parenchyma
$\xi = 0$
17 th generation
Diaphragm

Fig. 1

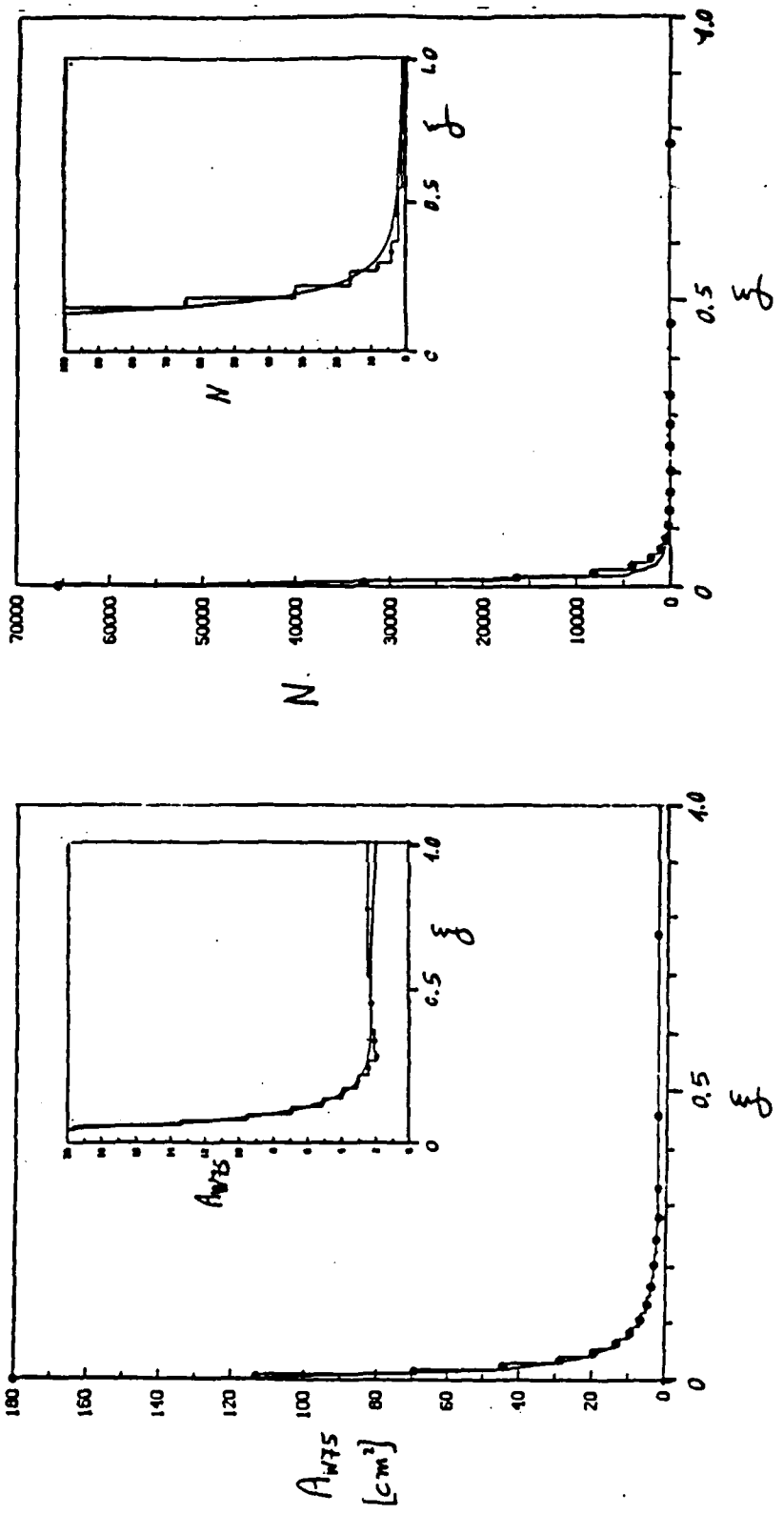
N
70000
60000
50000
40000
30000
20000
10000
0
0.5
1.0
ξ
N
0
0.5
1.0
ξ
A_{W75} [cm²]
180
160
140
120
100
80
60
40
20
0
0.5
1.0
ξ
A_{W75}
0
0.5
1.0
ξ

Fig. 2

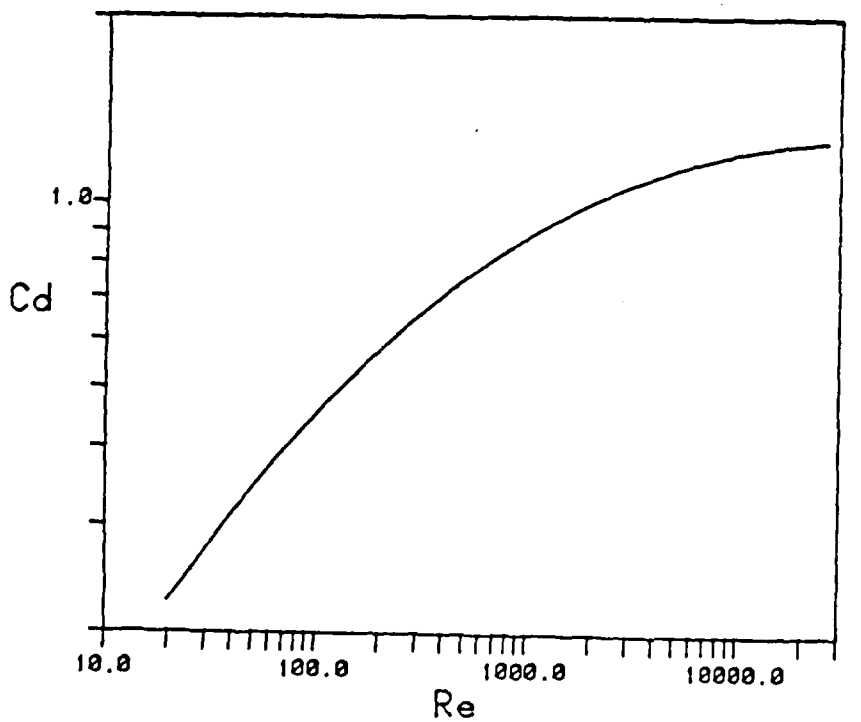

Fig. 3

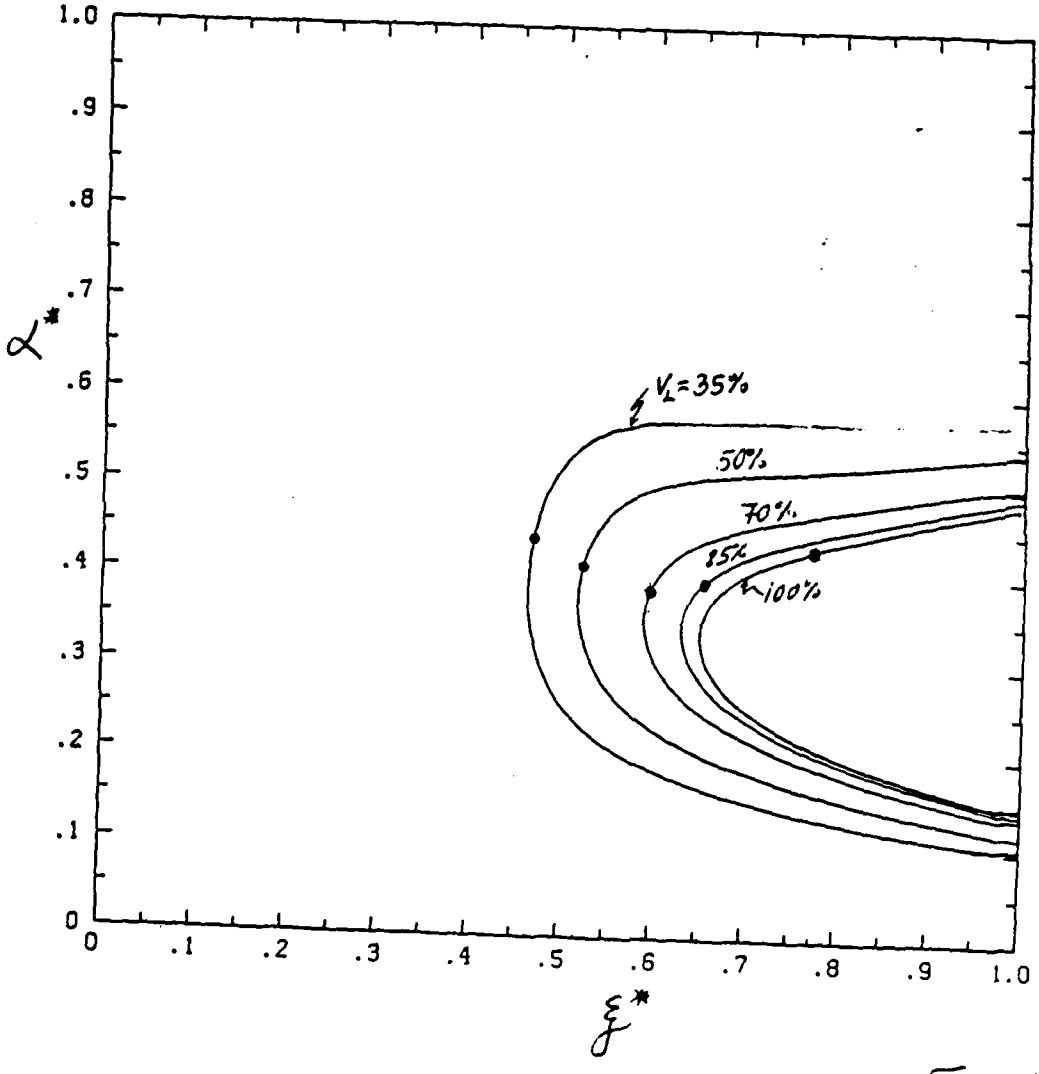
1.0
.9
.8
.7
.6
.5
.4
.3
.2
.1
0
0
.1
.2
.3
.4
.5
.6
.7
.8
.9
1.0
$\mathcal{L}^*$
$\mathcal{E}^*$
V_L=35%
50%
70%
85%
100%

Fig. 4

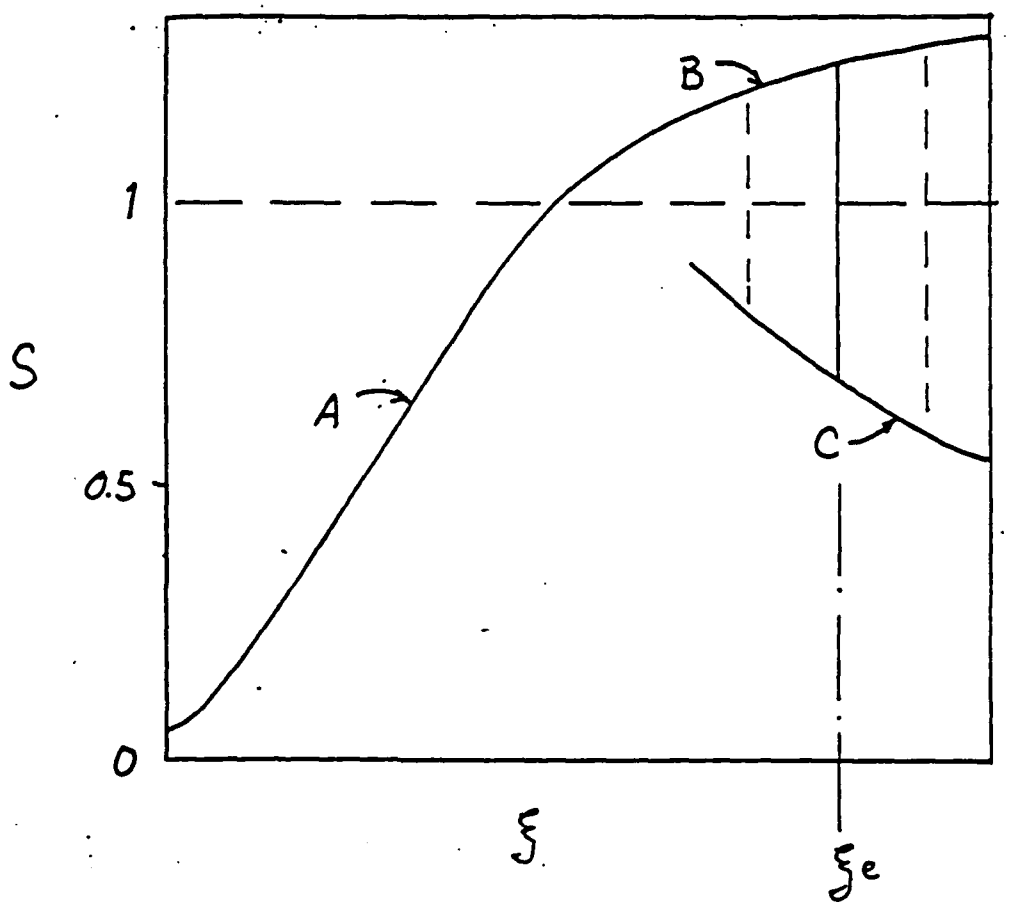

Fig. 4(b)

Uniform External Pressure

$f_T = \frac{16}{R_e}(a + bR_e)$

8/16/8

Model

	a	b	C_K
+	1.5	0.0013	2.40
×	1.5	0.0010	2.40
Δ	1.5	0.0014	2.40
o	1.5	0.0013	3.00
□	1.5	0.0013	(2.40)
*	1.5	0.0035	2.40

Reynolds (1920)

Experimental

●	Human (JB) Mea... et al (19...
■	Dog (#3) Mackl... et al (19...

generation	ξ
1	0.548 – 1.00
2	0.369 – 0.548
3	0.303 – 0.369
4	0.253 – 0.303
5	0.2248 – 0.253

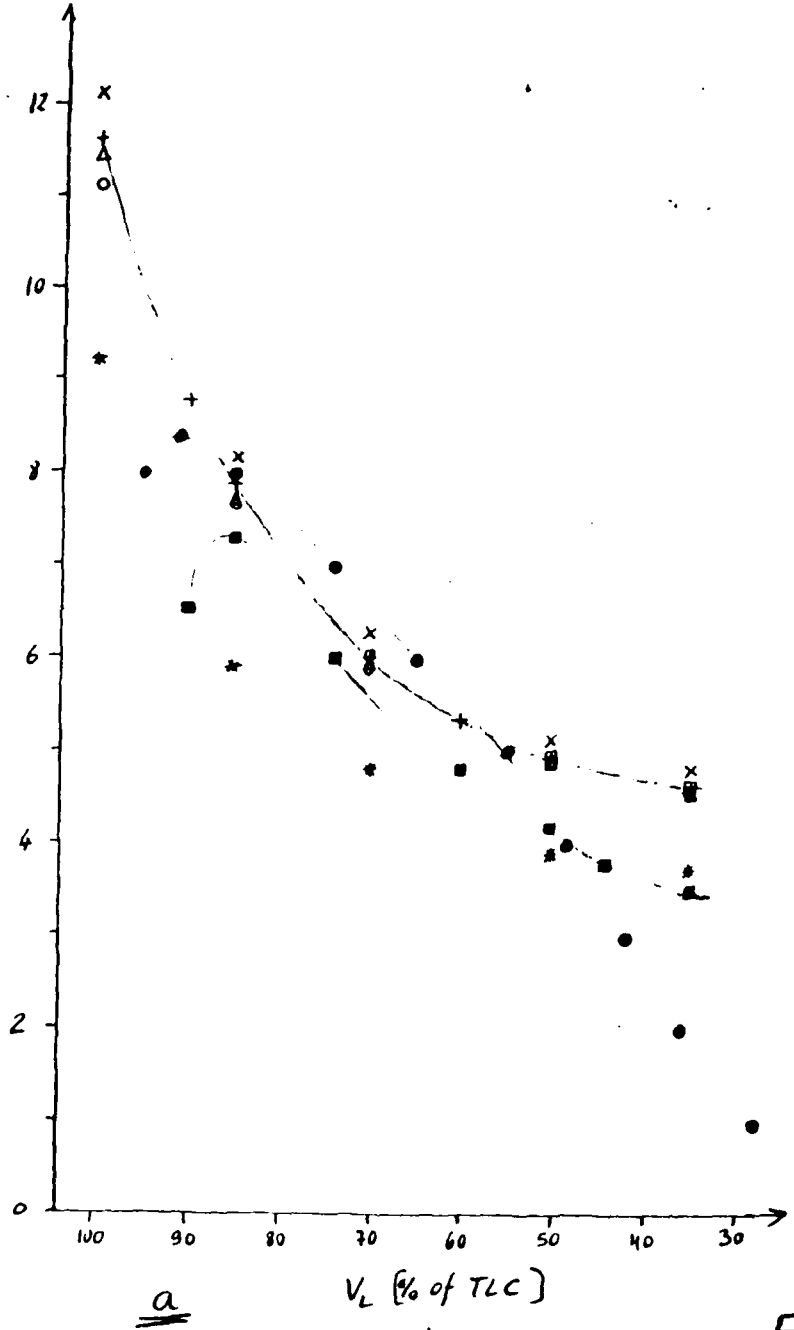

a

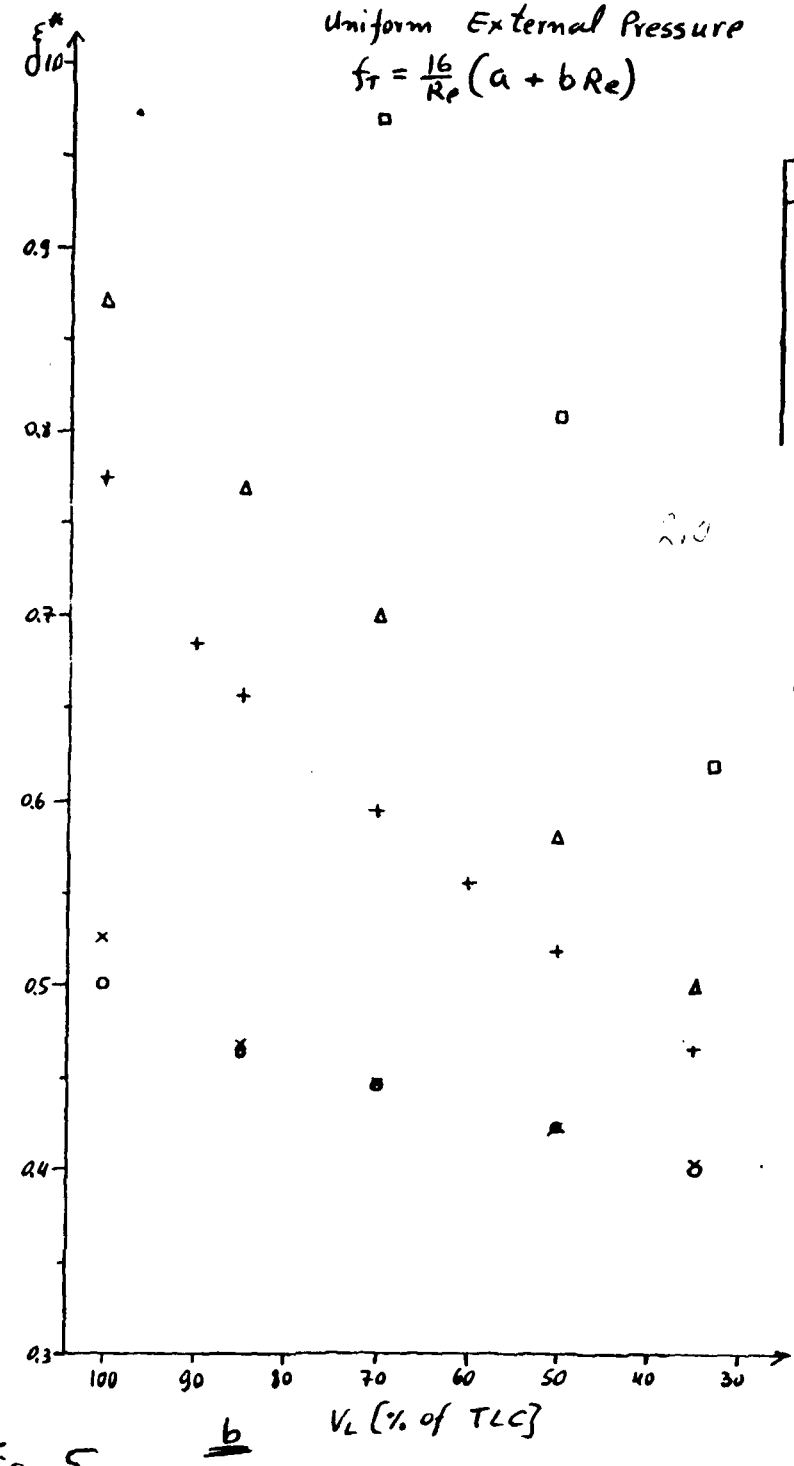

b

Fig. 5

$V_L = 60$

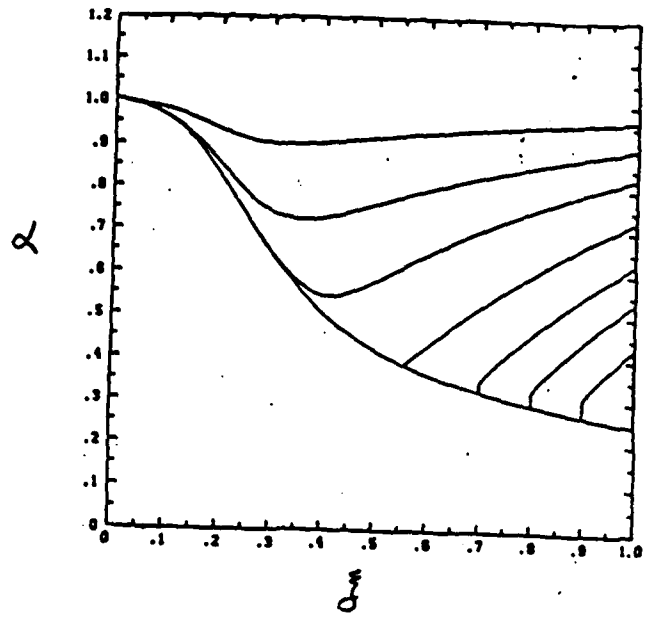

a

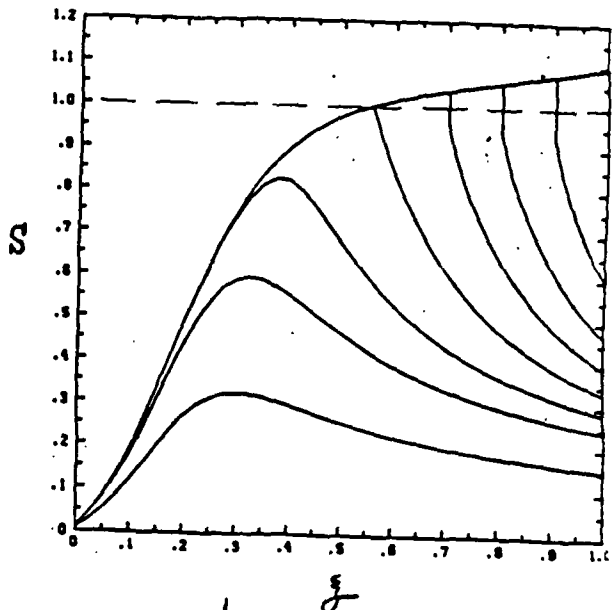

b

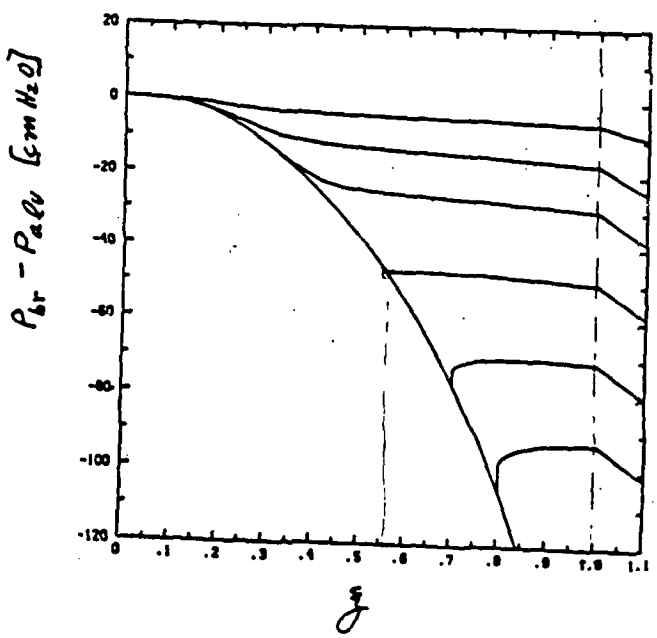

c

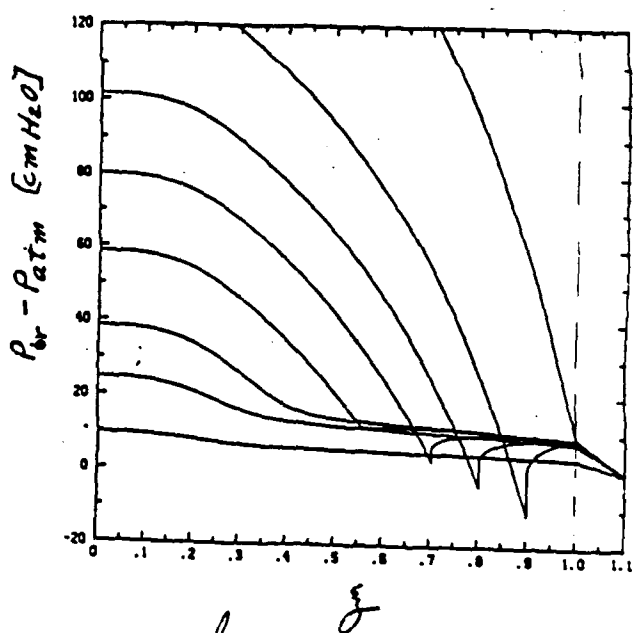

d

Fig. 6

8/20/85

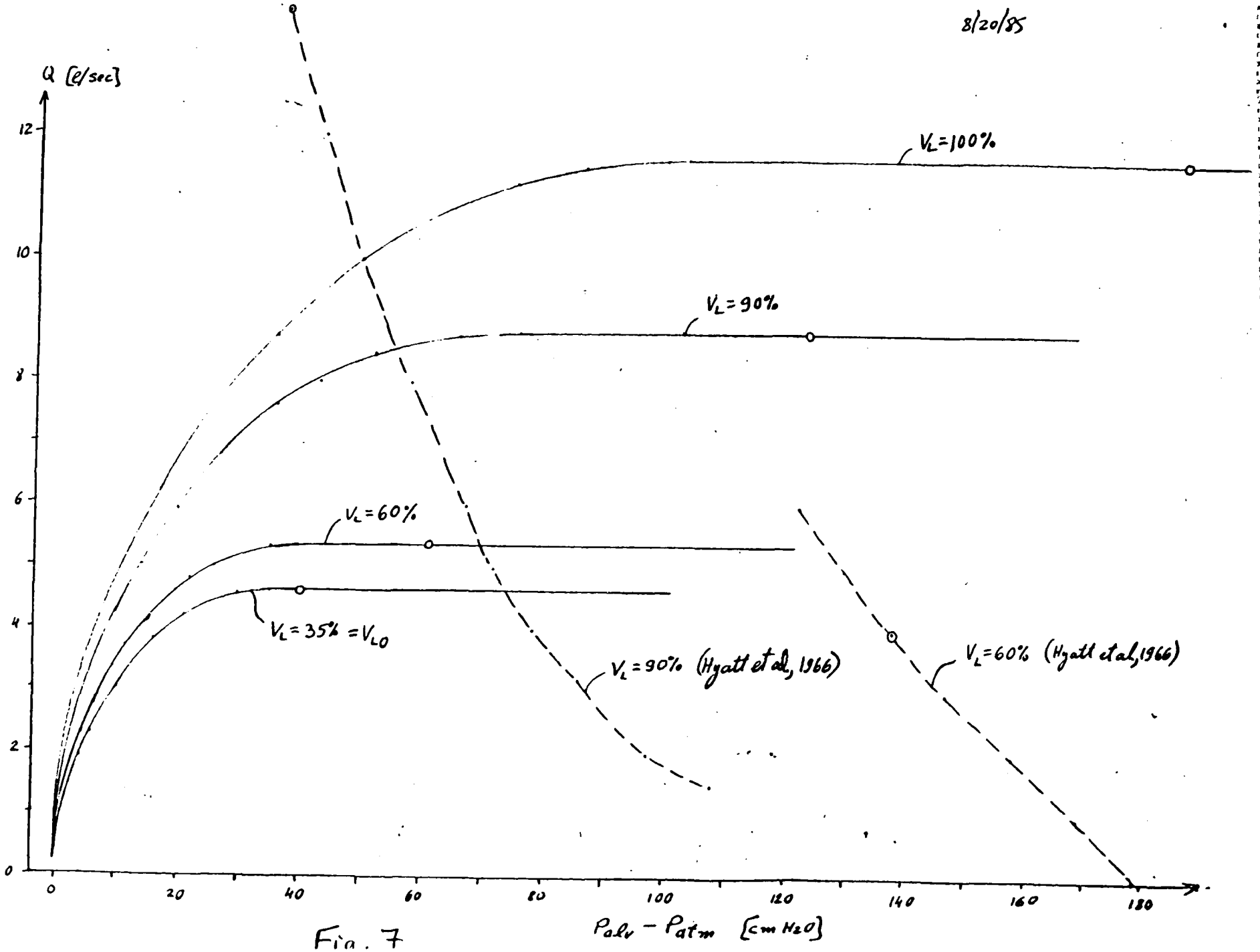
Q [ℓ/sec]
12
10
8
6
4
2
0
V_L=100%
V_L=90%
V_L=60%
V_L=35% =V_{LO}
V_L=90% (Hyatt et al, 1966)
V_L=60% (Hyatt et al, 1966)
0
20
40
60
80
100
120
140
160
180
$P_{alv} - P_{atm}$ [cm H_2O]

Fig. 7

8/16/85

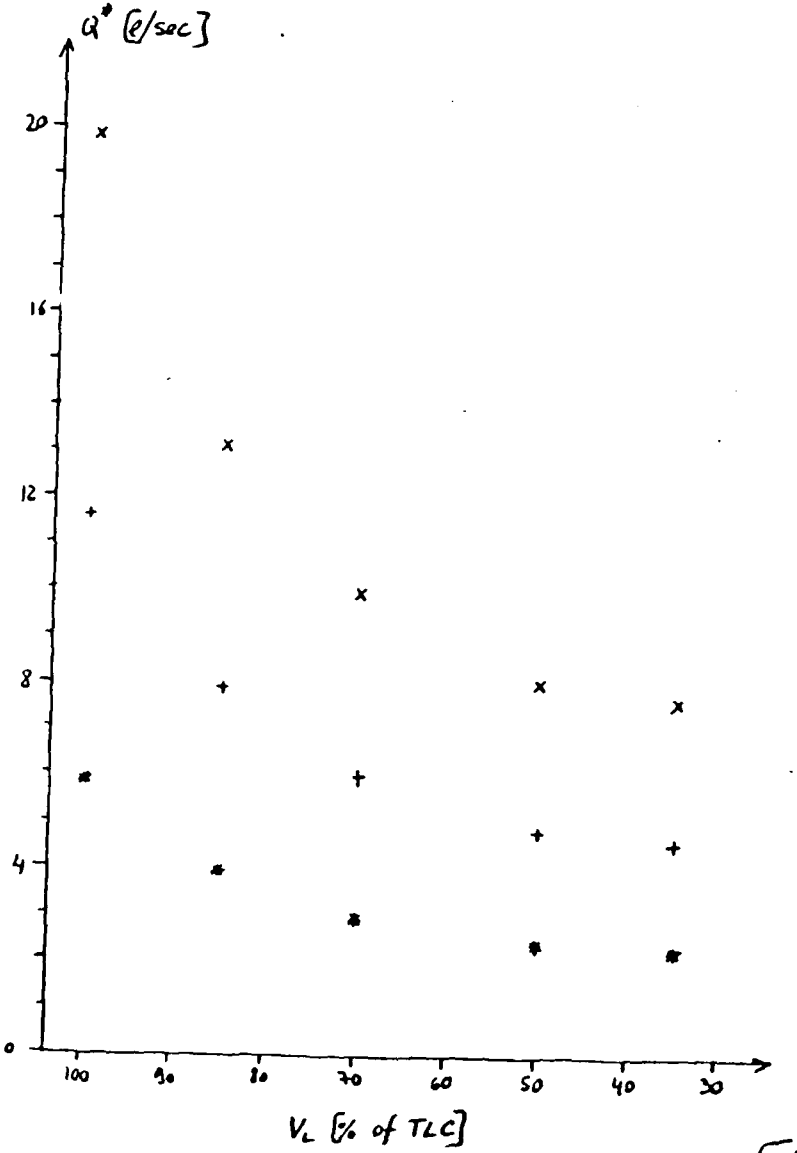

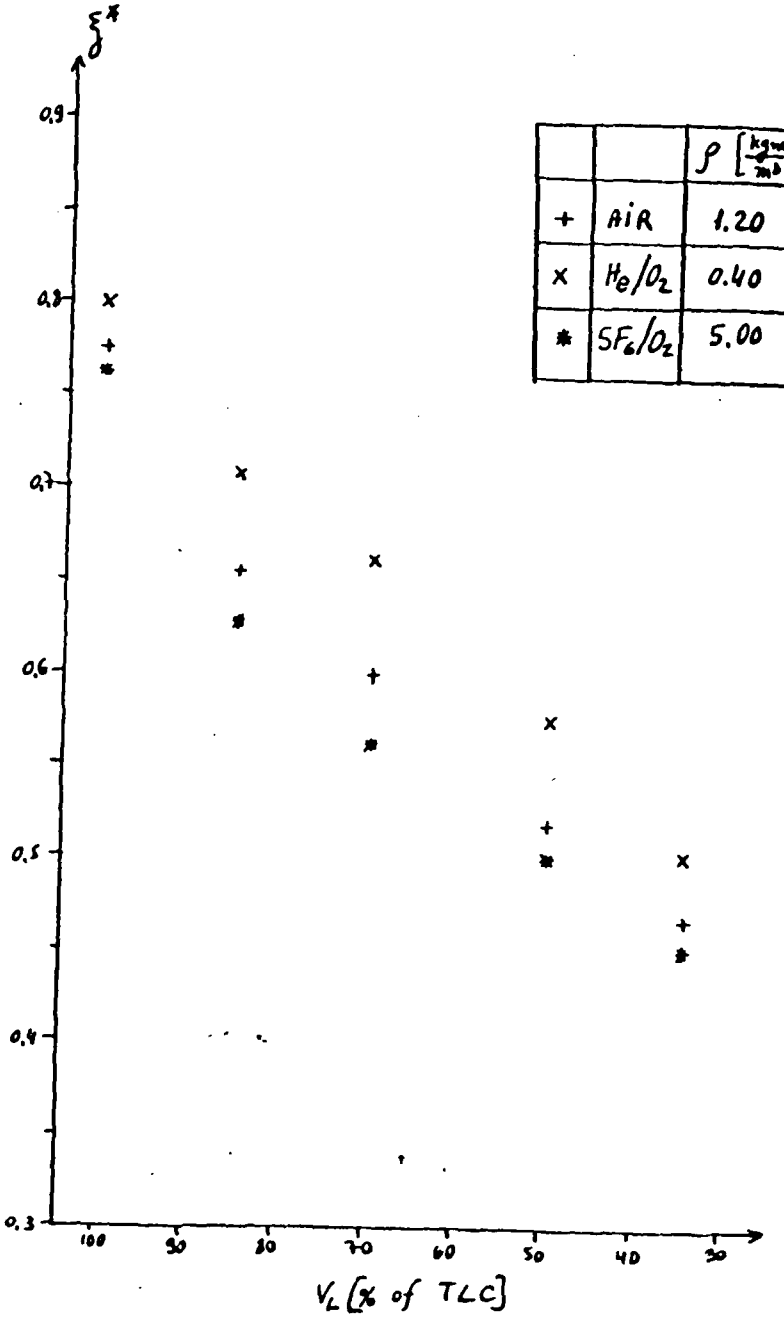

		$\rho \left[\frac{kg_m}{m^3}\right]$	$\nu \left[\frac{cm^2}{sec}\right]$
+	AIR	1.20	0.15
×	He/O_2	0.40	0.53
*	SF_6/O_2	5.00	0.03

Fig. 9

8/16/85

	C_K	a	b
AIR			
○	2.4	1.5	0.0013
△	2.4	1.5	0.0010
□	2.4	1.5	0.0014
He/O_2			
●	2.4	1.5	0.0013
SF_6/O_2			
▲	2.4	1.5	0.0013

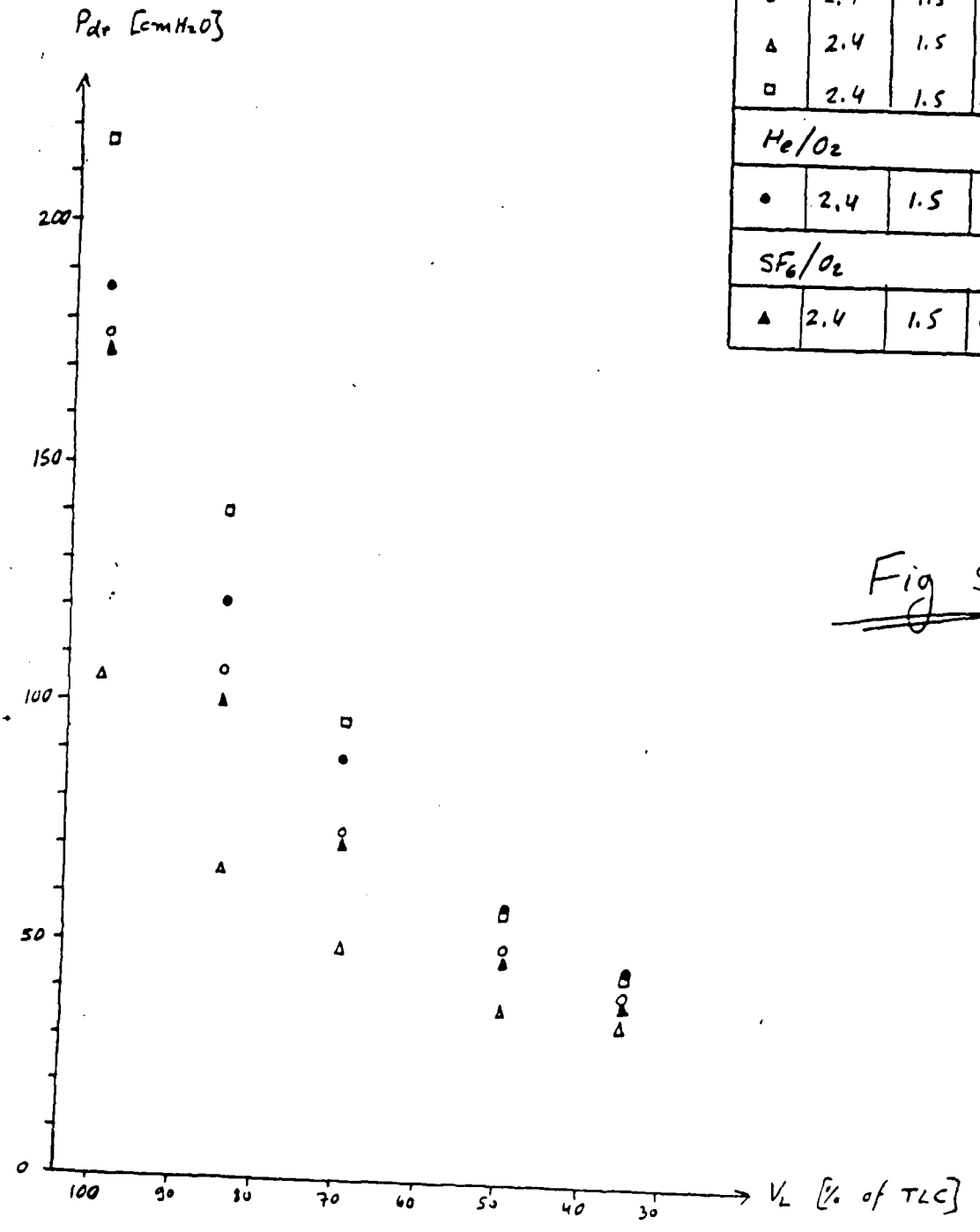

Fig 9

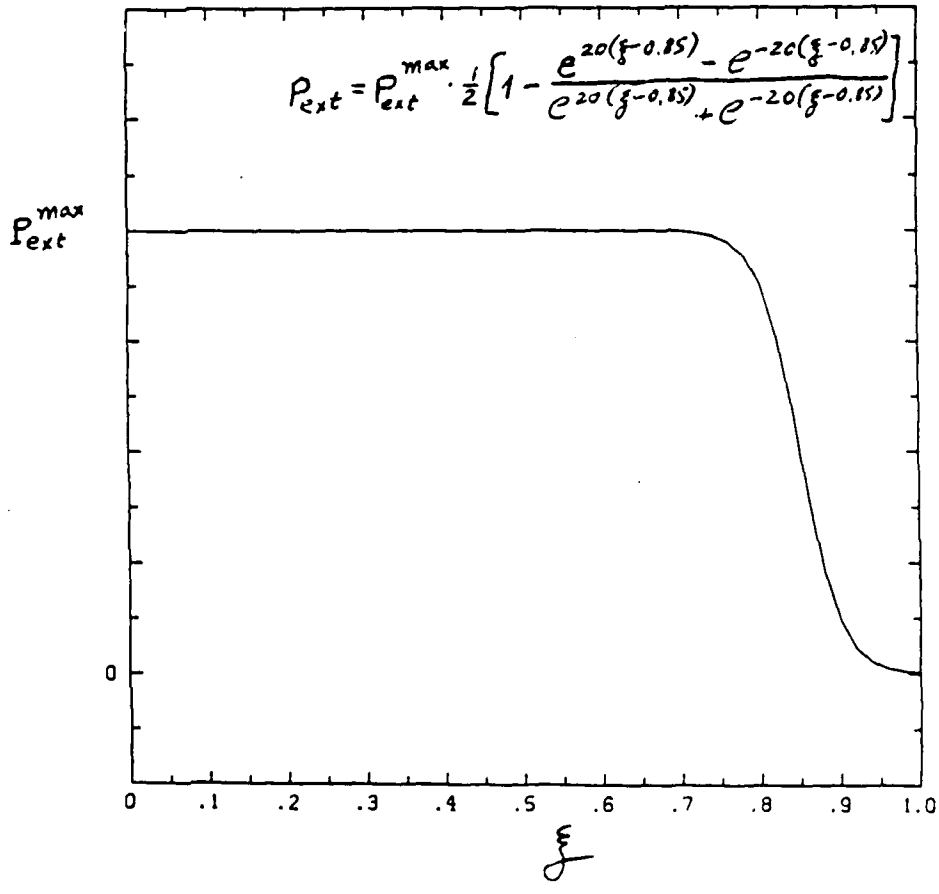
$P_{ext} = P_{ext}^{max} \cdot \frac{1}{2}\left[1 - \frac{e^{20(\xi-0.85)} - e^{-20(\xi-0.85)}}{e^{20(\xi-0.85)} + e^{-20(\xi-0.85)}}\right]$
P_{ext}^{max}
0
0
.1
.2
.3
.4
.5
.6
.7
.8
.9
1.0
ξ

Fig. 10

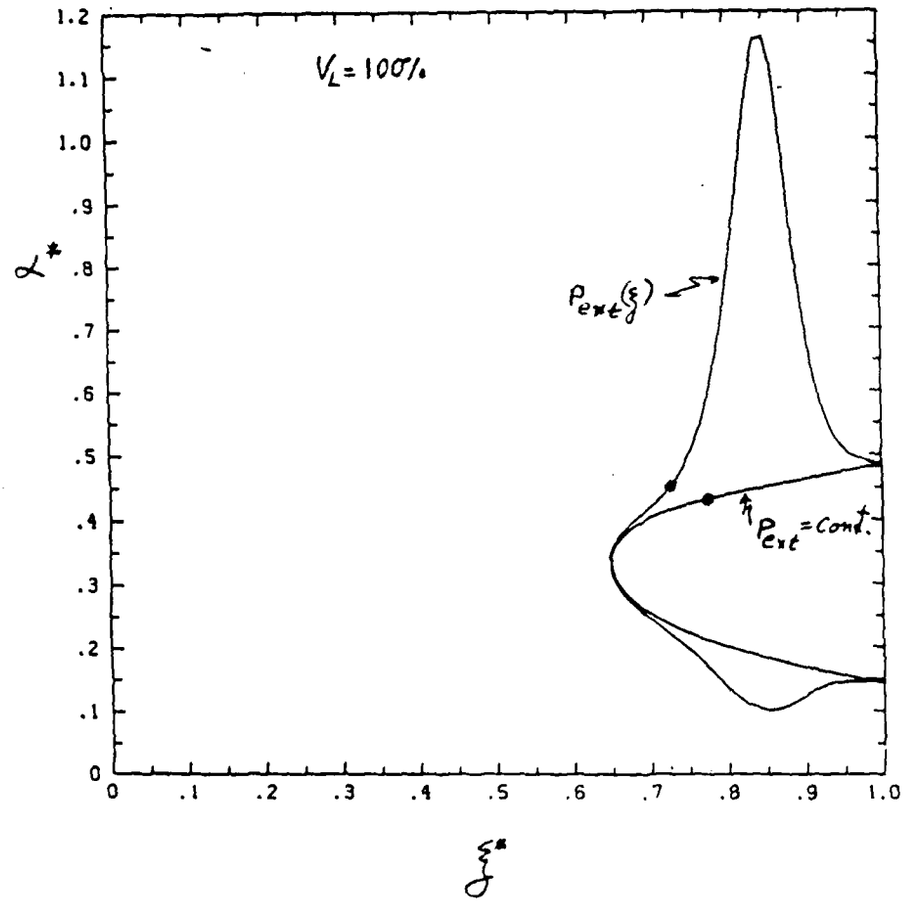

Fig. 11

8/16/85

FIGURE 12

a	b	C_K	P_e=Const.	P_e=f(ξ)
1.5	0.0013	2.40	o	●
1.5	0.0014	2.40	Δ	▲

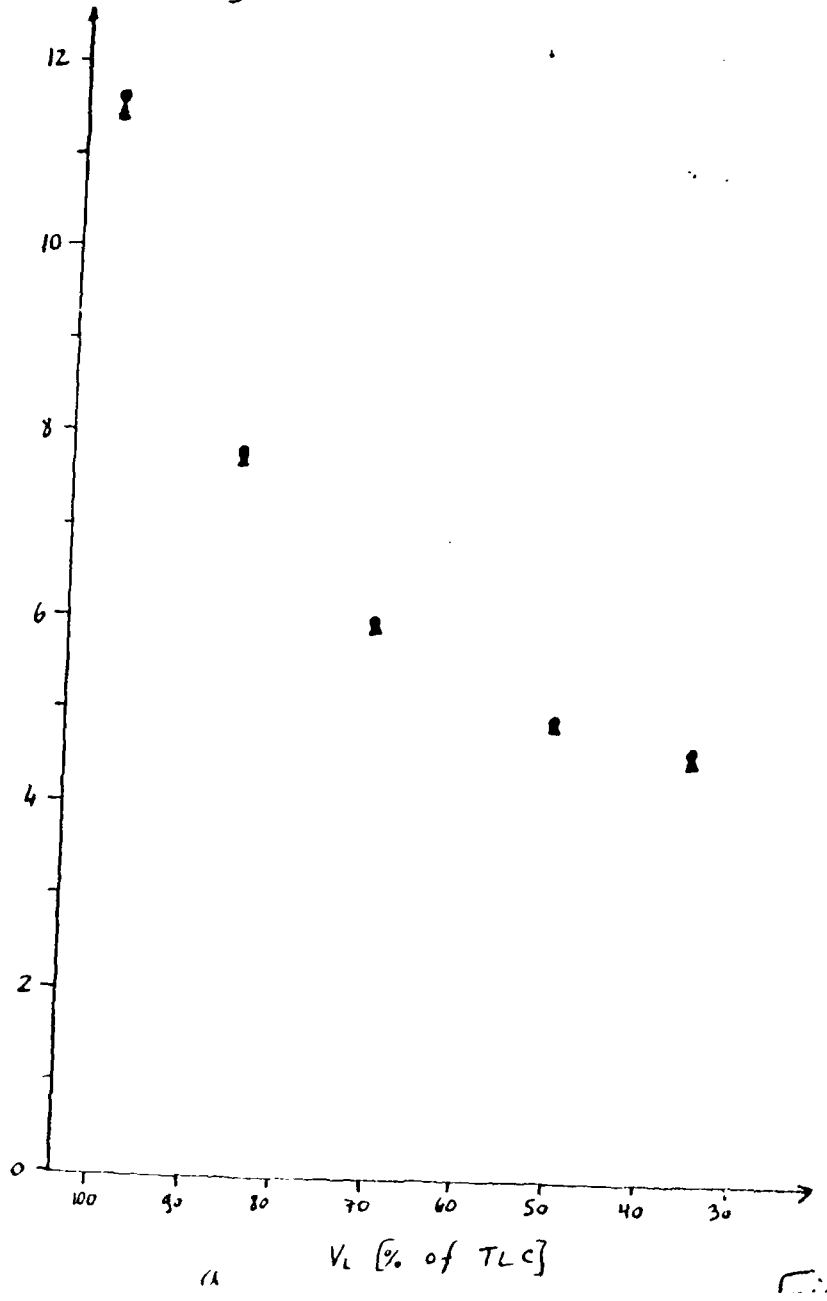

(a)

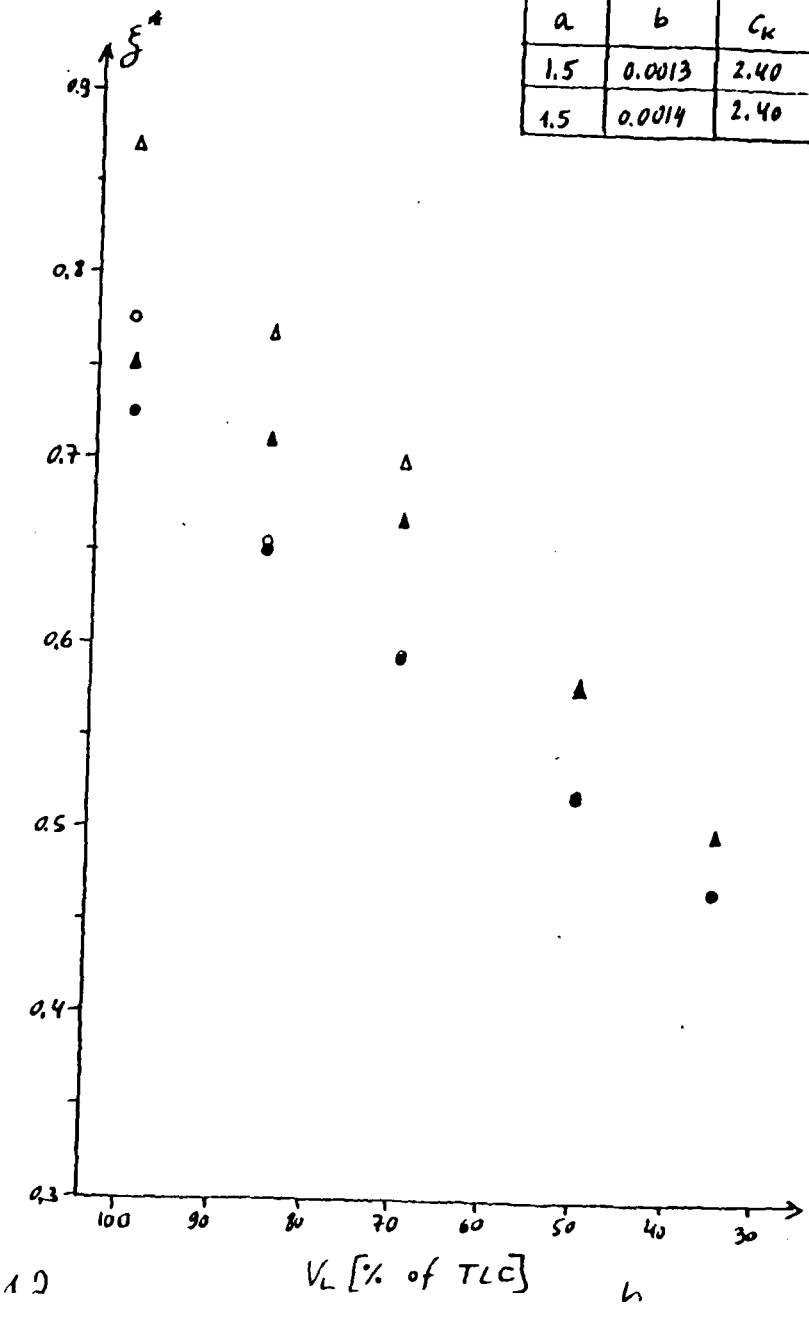

(b)

Fig. 12

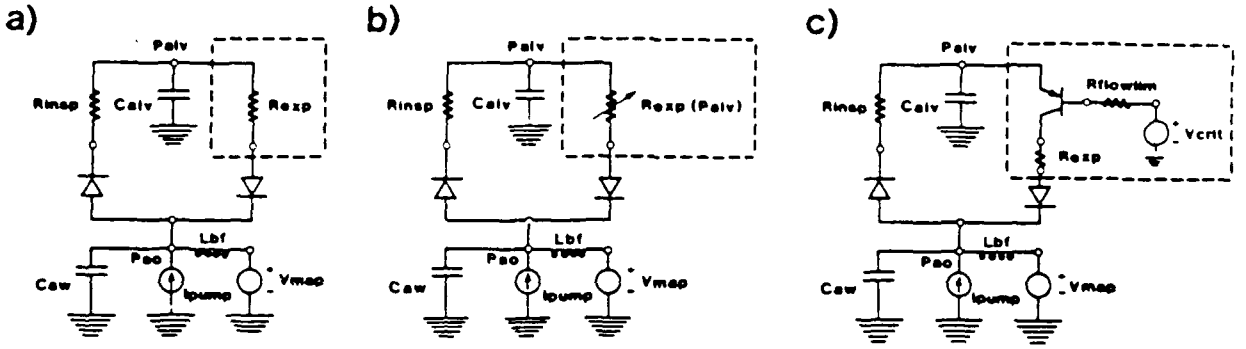
a)
Palv
Rinap
Calv
Rexp
Lbf
Paa
Caw
Ipump
Vmap
b)
Palv
Rinap
Calv
Rexp (Palv)
Lbf
Paa
Caw
Ipump
Vmap
c)
Palv
Rinap
Calv
Rflowlim
Vcrit
Rexp
Lbf
Paa
Caw
Ipump
Vmap

Figure 13

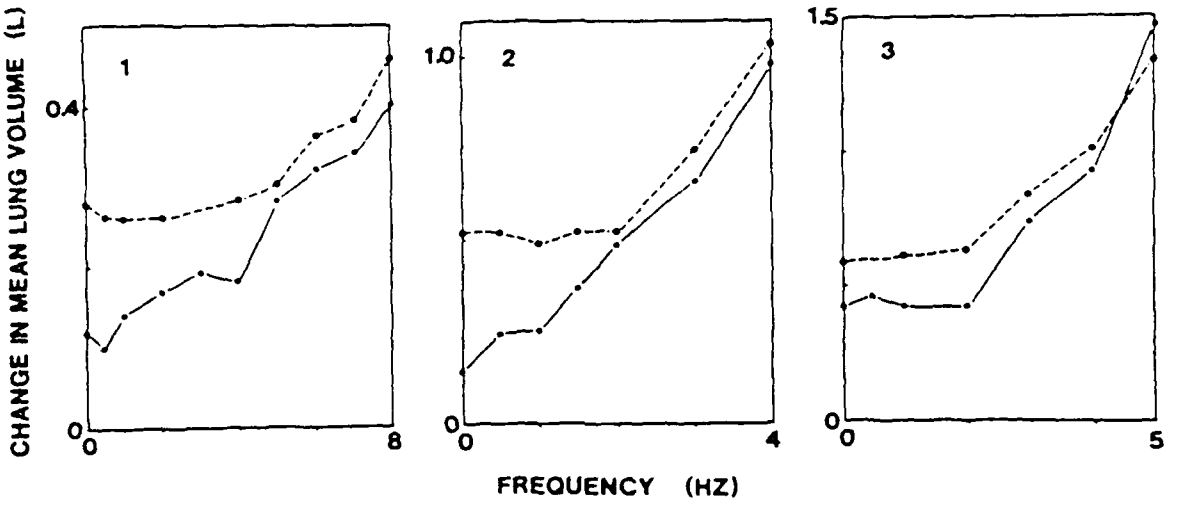
CHANGE IN MEAN LUNG VOLUME (L)
0.4
0
1
0
8
1.0
0
2
0
4
1.5
0
3
0
5
FREQUENCY (HZ)

Figure 14

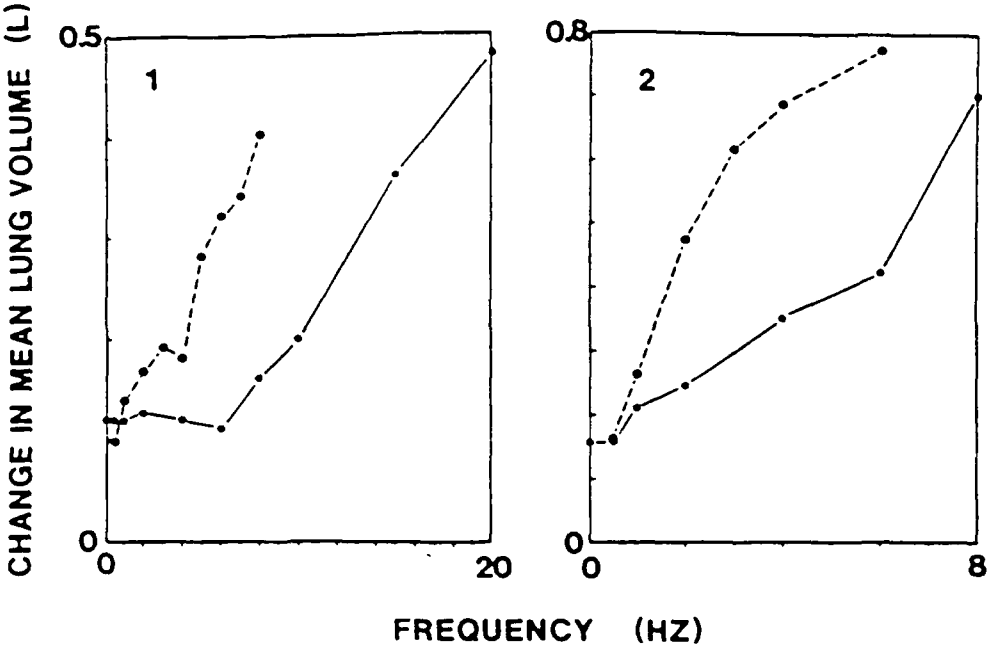

Figure 15

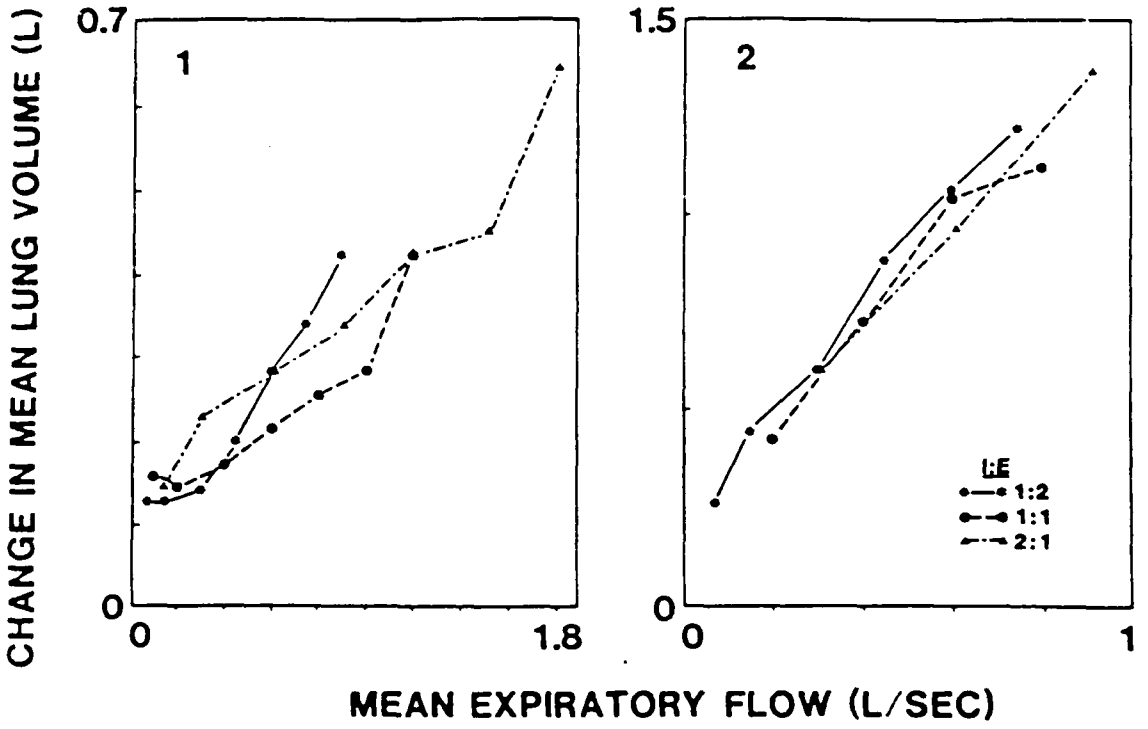
CHANGE IN MEAN LUNG VOLUME (L)
0.7
1
0
0
1.8
1.5
2
0
0
1
I:E
1:2
1:1
2:1
MEAN EXPIRATORY FLOW (L/SEC)

Figure 16

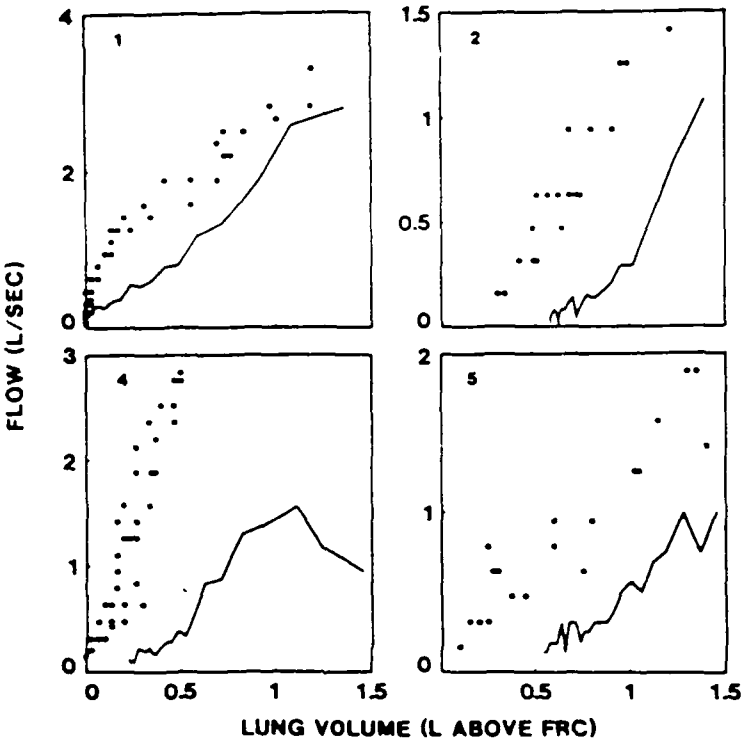

Figure 17

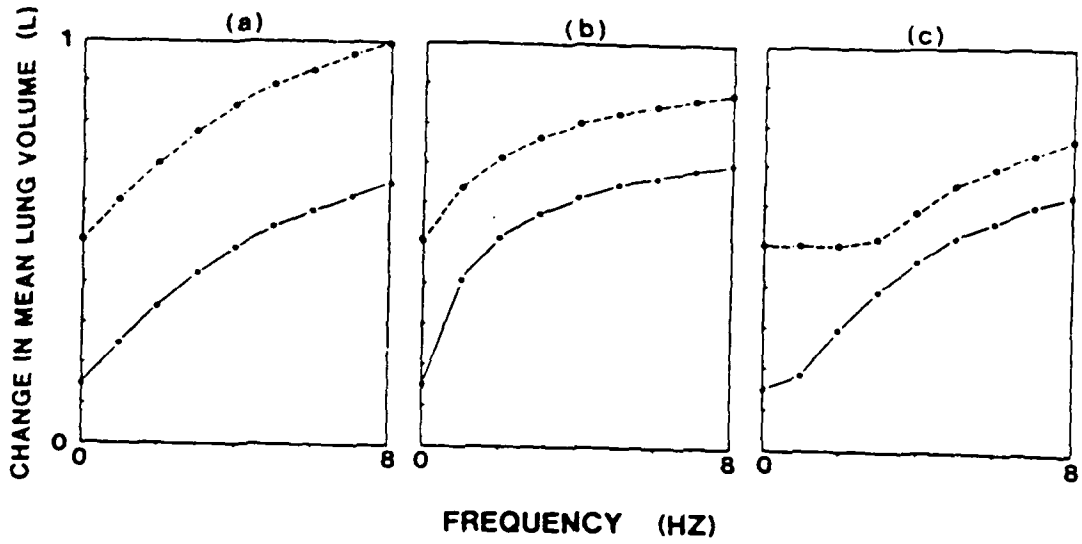

Figure 18

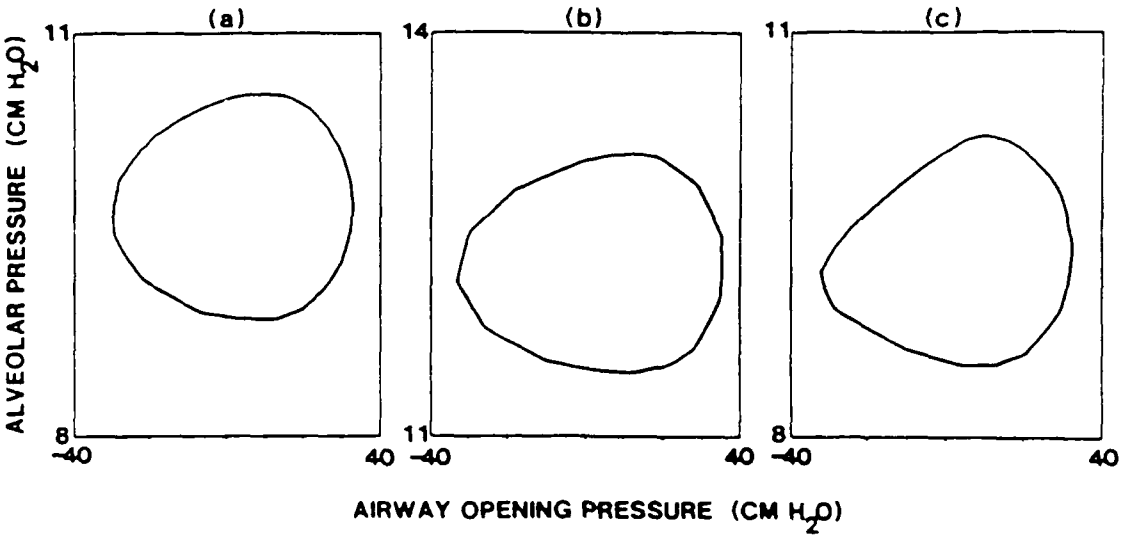
(a)
(b)
(c)
11
14
11
8
11
8
-40
40
-40
40
-40
40
ALVEOLAR PRESSURE (CM H2O)
AIRWAY OPENING PRESSURE (CM H2O)

Figure 19

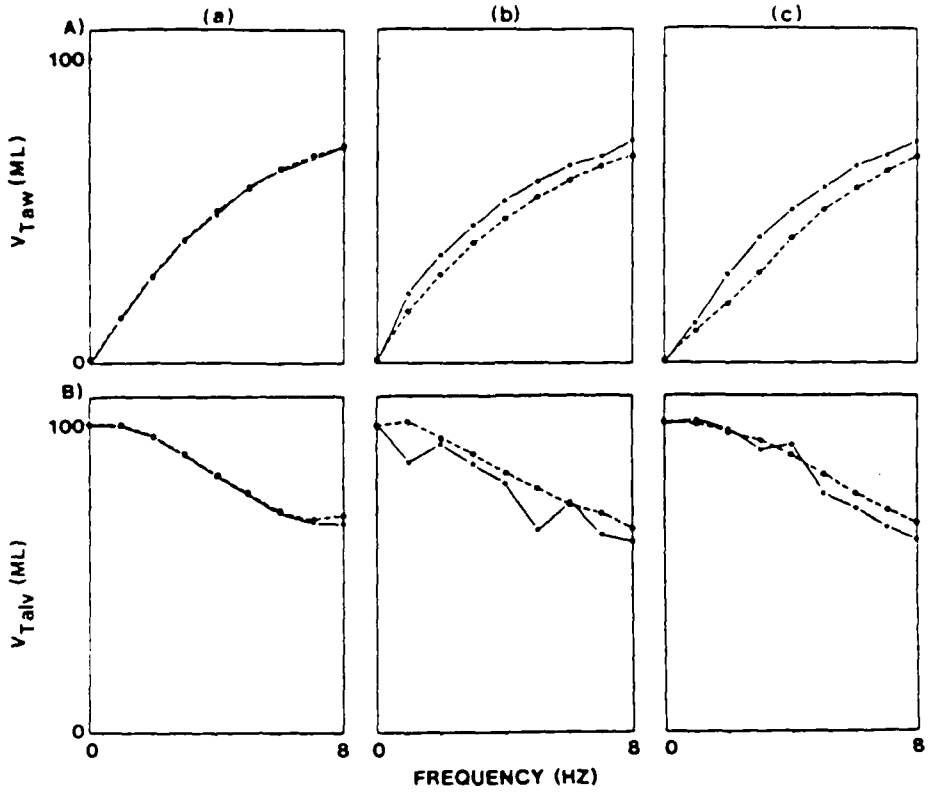

Figure 20

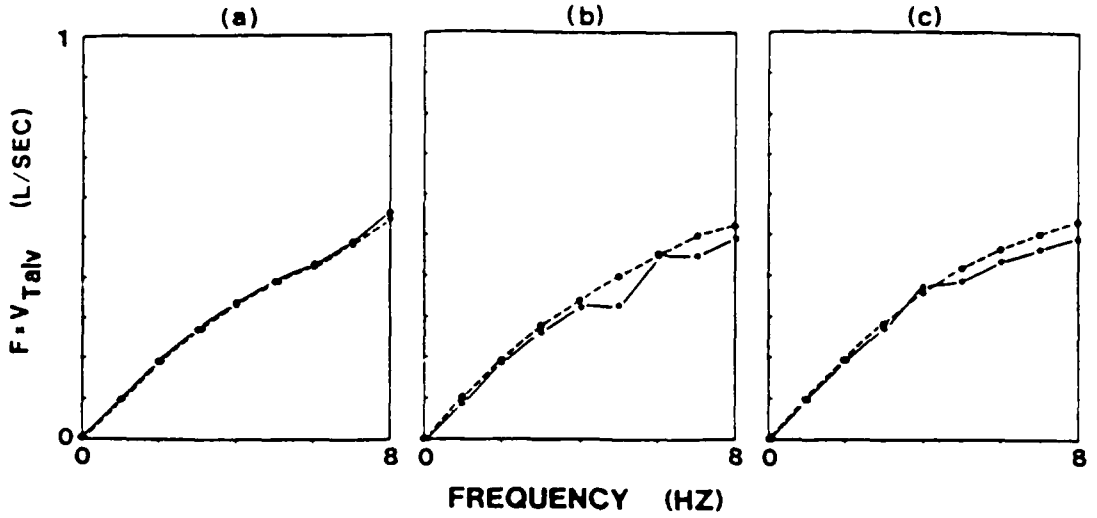

Figure 21

END

DATE

FILMED

DTIC

JULY 88